AD-A153 461 A SIMULATION STUDY OF JAMMER NULLING TRADE-OFFS IN A REACTIVELY STEERED ADAPTIVE ARRAY(U) NAVAL WEAPONS CENTER CHINA LAKE CA R J DINGER FEB 85 NWC-TP-6611 1/1

UNCLASSIFIED SBI-AD-E900 450 F/G 9/5 NL

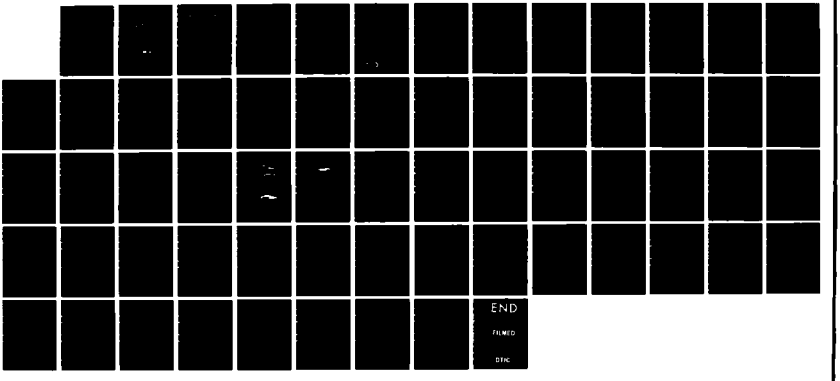

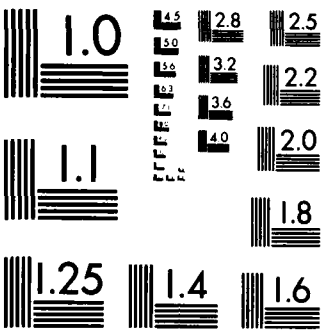

(2)

NWC TP 6611

AD-A153 461

A Simulation Study of Jammer Nulling Trade-Offs in a Reactively Steered Adaptive Array

by
Robert J. Dinger
Research Department

FEBRUARY 1985

NAVAL WEAPONS CENTER
CHINA LAKE, CA 93555-6001

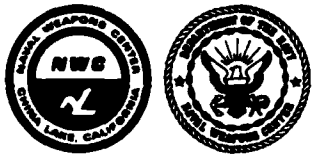

Approved for public release; distribution is unlimited.

Naval Weapons Center
AN ACTIVITY OF THE NAVAL MATERIAL COMMAND

FOREWORD

Antenna arrays that operate at frequencies up to 6 GHz or so on air-launched guided missiles are necessarily compact because of limited space. Research has been in progress since FY82 on a compact adaptive array that uses reactively loaded parasitic elements for pattern control. This report describes a study of this class of array whose purpose is to examine the trade-offs available among number of elements, element spacing, and number of nullable jammers. The research is part of a continuing effort to explore novel radio frequency radiating and receiving structures for application to airborne communications and radar system.

The research described in this report was performed during FY84. It was supported primarily by the Office of Naval Research, with some additional funding from the Independent Research program.

David J. White has reviewed the report for technical accuracy.

Approved by
E. B. ROYCE, Head
Research Department
25 February 1985

Under authority of
K. A. DICKERSON
Capt., USN
Commander

Released for publication by
B. W. HAYS
Technical Director

NWC Technical Publication 6611

Published by . . . . . .Technical Information Department
Collation . . . . . .Cover, 30 leaves
First printing . . . . . .120 copies

UNCLASSIFIED

SECURITY CLASSIFICATION OF THIS PAGE (When Data Entered)

REPORT DOCUMENTATION PAGE		READ INSTRUCTIONS BEFORE COMPLETING FORM
1. REPORT NUMBER NWC TP 6611	2. GOVT ACCESSION NO. AD-A153461	3. RECIPIENT'S CATALOG NUMBER
4. TITLE (and Subtitle) A Simulation Study of Jammer Nulling Trade-Offs in a Reactively Steered Adaptive Array		5. TYPE OF REPORT & PERIOD COVERED Interim report on continuing problem. 6. PERFORMING ORG. REPORT NUMBER
7. AUTHOR(s) Robert J. Dinger		8. CONTRACT OR GRANT NUMBER(s)
9. PERFORMING ORGANIZATION NAME AND ADDRESS Naval Weapons Center China Lake, CA 93555-6001		10. PROGRAM ELEMENT, PROJECT, TASK AREA & WORK UNIT NUMBERS 61153N; 61152N
11. CONTROLLING OFFICE NAME AND ADDRESS Naval Weapons Center China Lake, CA 93555-6001		12. REPORT DATE February 1985 13. NUMBER OF PAGES 56
14. MONITORING AGENCY NAME & ADDRESS(if different from Controlling Office)		15. SECURITY CLASS. (of this report) UNCLASSIFIED 15a. DECLASSIFICATION/DOWNGRADING SCHEDULE

16. DISTRIBUTION STATEMENT (of this Report)

Approved for public release; distribution is unlimited.

17. DISTRIBUTION STATEMENT (of the abstract entered in Block 20, if different from Report)

18. SUPPLEMENTARY NOTES

19. KEY WORDS (Continue on reverse side if necessary and identify by block number)

Adaptive Arrays
Anti-Jam Techniques
Optimization Techniques
Parasitic Antennas

20. ABSTRACT (Continue on reverse side if necessary and identify by block number)

See back of form.

DD FORM 1 JAN 73 1473 EDITION OF 1 NOV 65 IS OBSOLETE
S/N 0102-LF-014-6601

UNCLASSIFIED

SECURITY CLASSIFICATION OF THIS PAGE (When Data Entered)

(U) A Simulation Study of Jammer Nulling Trade-Offs in a Reactively Steered Adaptive Array, by Robert J. Dinger. China Lake, Calif., Naval Weapons Center, February 1985. 56 pp. (NWC TP 6611, publication UNCLASSIFIED.)

(U) The results of a computer simulation of the jammer nulling capability of a reactively steered adaptive array (RESAA) are presented. A RESAA consists of a single element connected to a receiver with parasitic elements mounted near this element. The parasitic elements are terminated in adjustable reactive terminations, and the pattern is formed according to the termination values. For the simulation, a symmetric linear array of center-fed half-wave dipoles has been assumed. The purposes of the simulation are to investigate the influence of element spacing on jammer rejection capability, to determine the number of jammers that can be nulled as a function of the number of elements, and to determine the nulling bandwidth. Both a power inversion (PI) mode, which assumes no desired signal is present, and a desired signal (DS) mode, which attempts to maintain a maximum antenna pattern response towards an incident desired signal, have been investigated.

(U) For three-, five-, and seven-element arrays controlled by the DS mode, each pair of degrees of freedom permits one jammer to be nulled. However, in adding two elements to go from a seven- to a nine-element array, two degrees of freedom are not added, presumably because the additional elements are too far from the driven element to have sufficient mutual coupling and, therefore, to contribute to control of the antenna pattern. In the PI mode, at most only two jammers could be nulled. As a function of element spacing, the jammer nulling ability showed a well-defined and consistent peak at spacings in the interval of 0.15 to 0.25 (λ = wavelength). The nulling bandwidth was found to be about 0.2 to 0.3 percent and was independent of the number of elements. All training of the arrays was performed on monochromatic jammers; training on jammers with a finite bandwidth would probably produce a larger nulling bandwidth. The results indicate that the RESAA technique is restricted to a relatively small number of elements (nine or less in a linear array) but performs well for small element spacings usually considered deleterious for conventional adaptive arrays.

SUMMARY

In this report we present the results of a computer simulation of the jammer nulling capability of a reactively steered adaptive array (RESAA). The configuration of a RESAA (shown in Figure 1) consists of a single element connected to a receiver, with parasitic elements mounted near this element. The parasitic elements are terminated in adjustable reactive terminations, and the pattern is formed according to the termination values. For the simulation, a symmetric linear array of center-fed half-wave dipoles has been assumed. The purposes of the simulation are to investigate the influence of element spacing on jammer rejection capability, to determine the number of jammers that can be nulled as a function of the number of elements, and to determine the nulling bandwidth. Both a power inversion (PI) mode, which assumes no desired signal is present, and a desired signal (DS) mode, which attempts to maintain a maximum antenna pattern response towards an incident desired signal, have been investigated.

Table 1 is a summary of the results. For three-, five-, and seven-element arrays controlled by the DS mode, each pair of degrees of freedom permits one jammer to be nulled. However, in adding two elements to go from a seven-element to a nine-element array, two degrees of freedom are not added, presumably because the additional elements (added to the ends of the array) are too far from the driven element to have sufficient mutual coupling and, therefore, to contribute to control of the antenna pattern. In the PI mode, at most only two jammers could be nulled; we believe this behavior results from a control surface that has more suboptimum minima, so that adaptive convergence to the best operating point is captured.

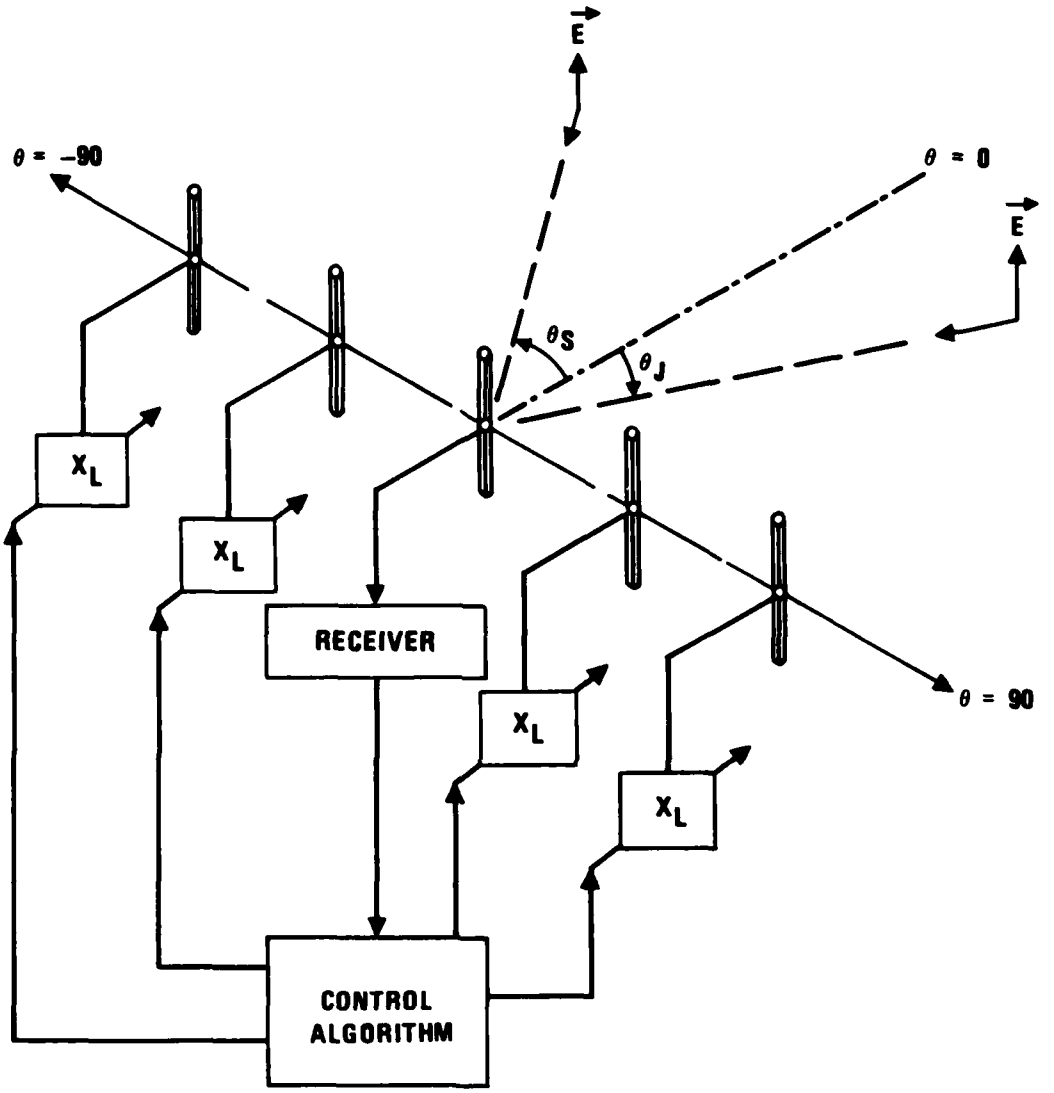

FIGURE 1. Reactively Steered Adaptive Array.

TABLE 1. Summary of Simulation Results.

Number of elements		3	5	7	9
Number of jammers that can be nulled	PI mode	1	2	2	2
	DS mode	1	2	3	3
Number of controlled variables (= apparent degrees of freedom)		2	4	6	8
Optimum element spacing (or range of spacings), wavelengths		0.1 (endfire) to 0.3 (broadside)	0.15 to 0.20	0.25	0.2
Nulling bandwidth (%)		0.2			

As a function of element spacing, the jammer nulling ability showed a well-defined and consistent peak at spacings in the interval of 0.15 to 0.25λ, where λ is the wavelength. Spacings smaller than this range produce a total radio frequency phase shift across the array aperture that is too small to permit good pattern control; spacings larger than this range cause the elements to have an insufficient mutual coupling.

The nulling bandwidth, defined as the frequency interval over which a particular "solution set" of reactive terminations maintains a -35 dB jammer rejection, was found to be about 0.2 to 0.3 percent. This range of values was found to be independent of the number of elements. All training of the arrays was performed on single frequency (tone) jammers. Training on jammers with a finite bandwidth would probably produce a larger nulling bandwidth.

The results indicate that the RESAA technique is restricted to a relatively small number of elements (nine or less in a linear array) but performs well for small element spacings usually considered deleterious for conventional adaptive arrays. These features, coupled with the simplicity of the hardware needed to implement a RESAA, suggest that the technique is useful for nulling two or three jammers on platforms whose size requires small element spacings (a ship at 5 MHz or a guided missile at 1 GHz).

INTRODUCTION

In two earlier reports (References 1 and 2), we have described the theory and measurements for a 4.0 GHz microstrip adaptive array that uses variable reactively terminated parasitic elements for control of the antenna pattern. Termed a reactively steered adaptive array (RESAA), the method uses only a single antenna element that is connected by a transmission line to the receiver. The closely coupled parasitic elements (spacing of one-tenth wavelength or so) act as loaded scatterers that reradiate to the receiver-connected element; the array summing occurs in the currents flowing on this element. Beam forming is possible because the phase of the scattered radiation is a function of the reactive termination value.

The emphasis in the earlier reports was on experimental data, with enough theory included to interpret the results. These experimental results (and earlier results (References 3 through 5) for a RESAA with vertical dipole elements operating at 20 MHz) have verified that a RESAA can steer a narrow, deep null towards a jammer, even with an interelement spacing of only one-tenth wavelength. However, a number of questions regarding the capability of the RESAA technique have not been addressed in these feasibility measurements. Some of these questions are:

- How many independent nulls can be steered for a given number of elements?
- How does the null depth and jammer rejection depend on the number of elements and their spacing?
- Is there an optimum spacing?
- Is there an optimum number of elements?
- How does the nulling bandwidth depend on element spacing and number of elements?

The purpose of this report is to describe the results of a computer simulation that addresses these questions. The answers for a conventional (fully driven) adaptive array are well known and in most

cases can be derived by analytical techniques. For a RESAA, however, the complexity of the equation for the antenna array factor does not permit a purely analytical study of RESAA performance. Therefore, the approach in this report is to use the array factor equation with a simulation of the control algorithm to compute array patterns and frequency response curves over a wide range of conditions. From these computed curves we attempt to draw as many conclusions as the results allow.

Although the experimental results (References 1 and 2) were taken on an array of microstrip rectangular patch elements, the numerical complexity of computing the entries in the mutual impedance matrix for these elements has forced us to assume a simpler element. We assume center-fed dipole elements and use the computer program given by Harrington and Mautz to evaluate the impedance matrix (Reference 6). Strictly speaking, this choice limits the conclusions of this study only to arrays of center-fed dipole elements; however, based on our observations of the similarity in behavior of a 4.0 GHz microstrip RESAA (References 1 and 2) and a 20 MHz dipole RESAA (References 3 through 5), we believe that the results in this report can safely be extended to a wide variety of elements and operating frequencies.

Below, following a discussion of the theory for the RESAA and its control algorithms, we present the results of the simulation. There are a variety of ways to arrange the presentation of the results, e.g., by number of jammers, by element spacing, or by number of elements. We have chosen the last approach: the number of elements is the major category, and for each number of elements, array performance for various numbers of jammers and element spacings is discussed.

THEORY

PATTERN EQUATION

Figure 1 is a diagram of a linear array of N center-fed dipoles with the center element connected (and matched) to a receiver and the other elements terminated by variable reactive loads. A signal and jammer are incident on the array as indicated. Harrington first analyzed such an array (References 6 and 7); as shown in Reference 1, his analysis leads to the following equation for the array pattern:

$$F(\theta) = g(\theta) \sum_{n=1}^{N} \{[Z_A + Z_L]^{-1}\}_{np} e^{jks(n-p)\cos\theta} \qquad (1)$$

where $g(\theta)$ is the element pattern, $(-)_{np}$ denotes the np element of the enclosed matrix, $p = (N+1)/2$ is the index for the center driven element, $k = 2\pi/\lambda$, s is the element spacing, $[Z_A]$ is the array impedance matrix, and $[Z_L]$ is the diagonal matrix of reactive loads given by

$$[Z_L] = \begin{bmatrix} X_{L_1} & & & & 0 \\ & X_{L_2} & & & \\ & & \ddots & & \\ & & & X_{L_{(p-1)}} & \\ 0 & & & & X_{L_{(p+1)}} \\ & & & & \ddots \\ & & & & X_{L_N} \end{bmatrix} \tag{2}$$

where X_{Li} is the reactive load on the ith element. It will be convenient to consider also the diagonal elements of $[Z_L]$ as a vector denoted by $\vec{X}_L$. For the calculations in this report, the signals are assumed to be incident on the array in the plane normal to the dipole axes and polarized as shown in Figure 1. Hence, the element factor is unity ($g(\theta) = 1.0$).

To proceed any further analytically with Equation 1, we must simplify the matrix inverse that appears in the equation. Unfortunately, there does not appear to be any simpler form, and we must resort to computer evaluation of Equation 1.

We define the current vector $\vec{I}$ with components

$$I_n = \{[Z_A + Z_L]^{-1}\}_{np} \tag{3}$$

and the steering vector $\vec{U}$ with components

$$U_n(\theta) = e^{jks(n-p)\cos\theta} \tag{4}$$

Then, for the general case of an incident desired signal and multiple jammers, the array output voltage is given by

$$P_o = P_s\left|\vec{I}\cdot\vec{V}(\theta_s)\right|^2 + \sum_{m=1}^{M} P_m\left|\vec{I}\cdot\vec{U}(\theta_{Jm})\right|^2 + N_o \tag{5}$$

where θ_S and P_S are the desired signal incidence angle and power, respectively; θ_{Jm} and P_m ($m = 1,M$) are the jammer incidence angles and powers, respectively; and N_o is the receiver noise power. The signal-to-jammer power ratio (SJR) is given by

$$SJR = \frac{P_S \left| \vec{I} \cdot \vec{V}(\theta_S) \right|^2}{\sum_{m=1}^{M} P_m \left| \vec{I} \cdot \vec{V}(\theta_{Jm}) \right|^2 + N_o} \tag{6}$$

Equations 5 and 6 were used as appropriate to calculate the array response for the curves presented below.

ARRAY IMPEDANCE MATRIX

We calculated $[Z_A]$ using the computer program given in Reference 6. This program uses equations for the mutual impedance derived by the induced electromotive force method with assumed sinusoidal current (Reference 8). As Harrington and Mautz show (Reference 6), this method agrees very closely with more accurate method-of-moment calculations, as long as the dipoles are a half wavelength or less in length. Figure 2 is a plot of the mutual impedance between two dipoles as determined by this computer program.

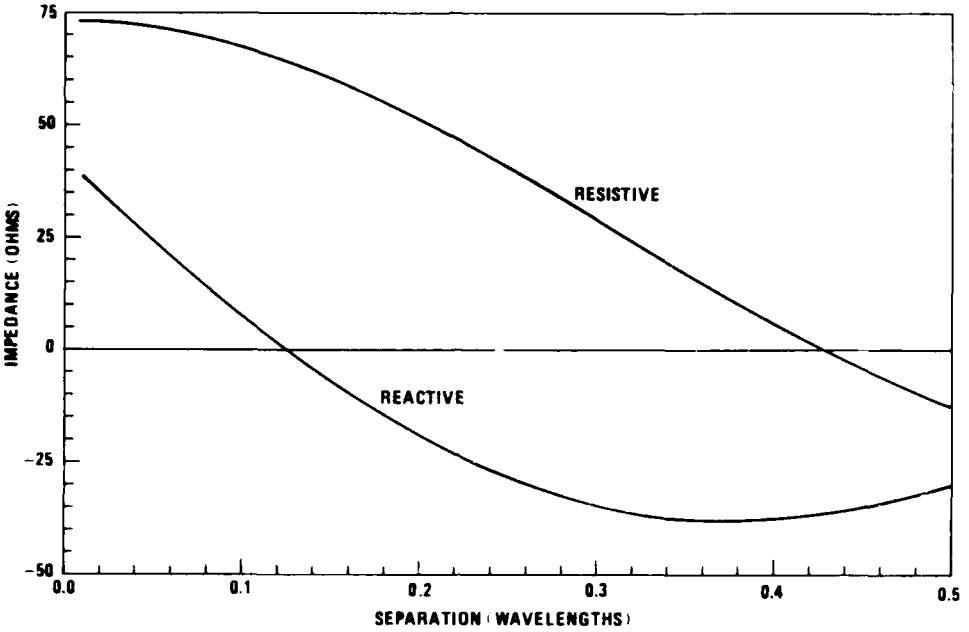

FIGURE 2. Mutual Impedance Versus Element Spacing as Calculated by Computer Program Used in Simulation. Dipole radius = 0.01λ; height = 0.5λ.

BEAM-FORMING ALGORITHMS

The adaptive control of a RESAA can be viewed as an optimization problem. If the objective is to null a single incident jammer, for example, the problem is to minimize

$$P_o = P_1 \left| \vec{I} \cdot \vec{V}(\theta_{J1}) \right|^2 \tag{7}$$

by adjustment of the X_{Li} in $[Z_L]$, subject to the condition that $X_{L\ell} < X_{Li} < X_{Lu}$, where $X_{L\ell}$ and X_{Lu} are hardware limits on the reactive loads. Because of the complicated dependence of P_o on the X_{Li} and because Equation 7 is only an approximation, practical adaptive control of a RESAA must use a method that is independent of any assumed relationship between array output and the X_{Li}.

Most such methods fall in either the gradient search or random search categories (Reference 9). However, there is a large variation in the complexity of the algorithms in these two classes. The algorithm used in Reference 2 for RESAA control is probably the simplest possible gradient algorithm possible; it was purposely kept simple for

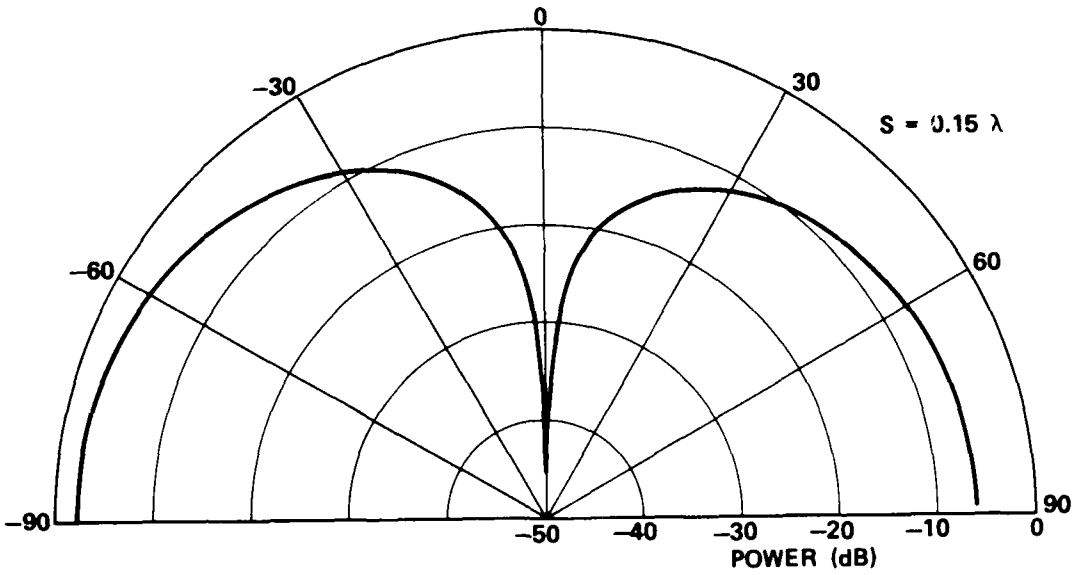

(b) Spacing = 0.15λ.

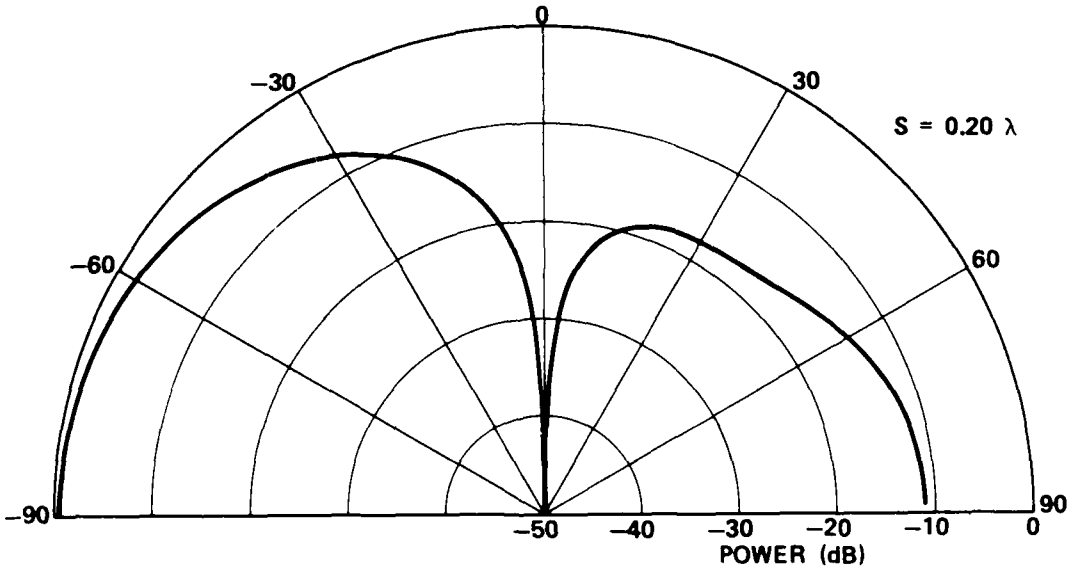

(c) Spacing = 0.20λ.

FIGURE 9. (Contd.)

Steady State Response. Figure 9 shows the antenna patterns after nulling by steepest descent for six different spacings varying from 0.05 to 0.35λ. In Figure 10 the depth and bandwidth of the null are plotted as a function of spacing. In Figure 11 the null frequency response is given for the six patterns shown in Figure 9; the bandwidth points in Figure 10 were taken from these curves.

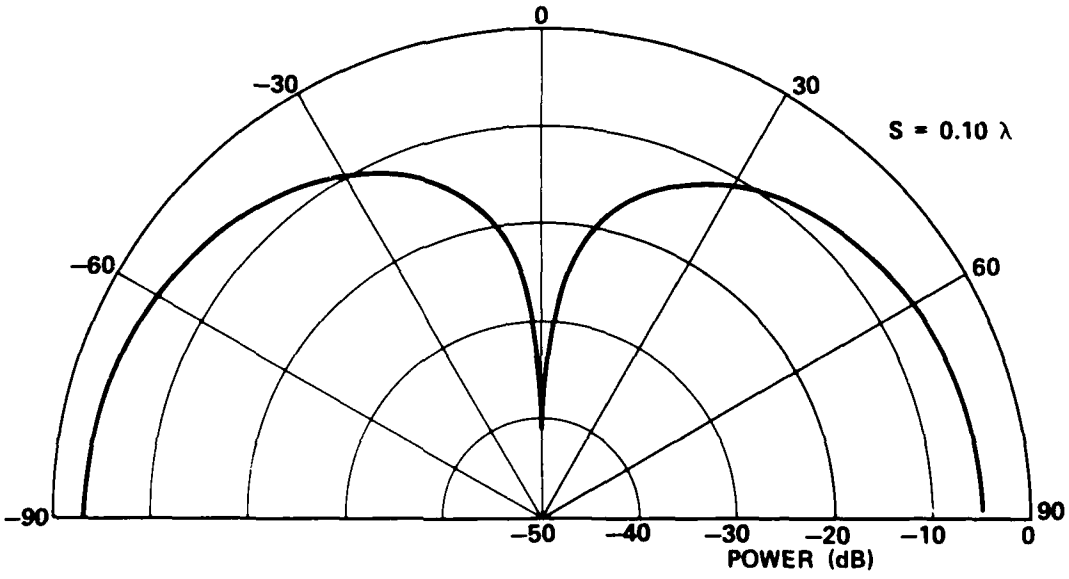

(a) Spacing = 0.10λ.

FIGURE 9. Antenna Patterns After Nulling by Steepest Descent for Six Element Spacings. Three-element array, PI mode control, jammer incident at 0 degrees.

As the result of a large number of simulation runs with various numbers of elements in both the PI mode and the DS mode, we found that the optimum value of K is given approximately by

$$K_{opt} = \frac{1}{2PN} \tag{12}$$

where P is the total incident power and N is the number of elements. The inverse dependence of K on the total received power is consistent with theory and experiment for conventional adaptive arrays that use gradient algorithms (Reference 12). The N in the denominator of Equation 12 appears because the parasitic elements couple (reflect) power to the main element, thus increasing the effective incident power.

Figure 8 shows the evolution of the antenna pattern for one of the sets of conditions used in Figure 6. Note that pattern seems to form a null initially at an azimuth of -2 degrees and then moves this null to 0 degrees.

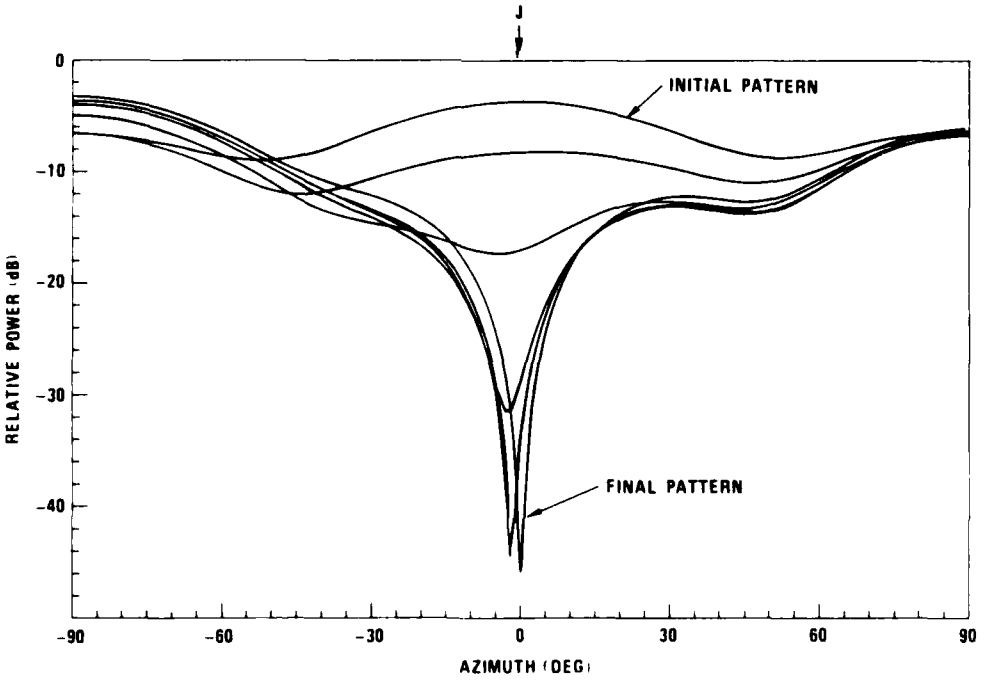

FIGURE 8. Patterns During Adaptation for a Three-Element Array Under PI Mode Control. Jammer incident at 0 degrees; $K = 3.0 \times 10^{-4}$.

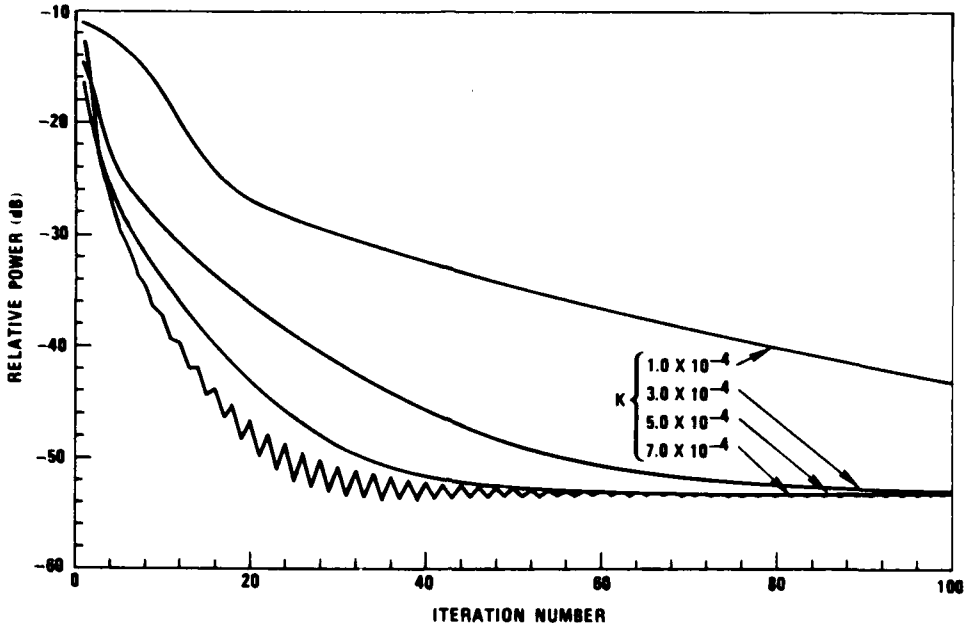

FIGURE 6. Transient Response with K as a Parameter for PI Mode Control.

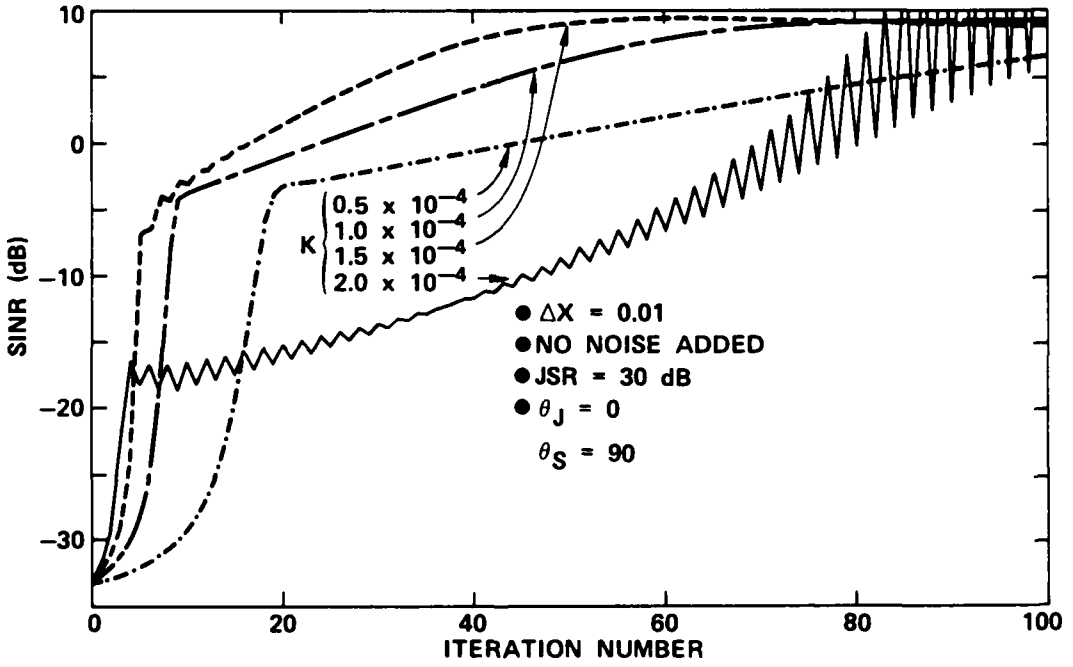

FIGURE 7. Transient Response with K as a Parameter.

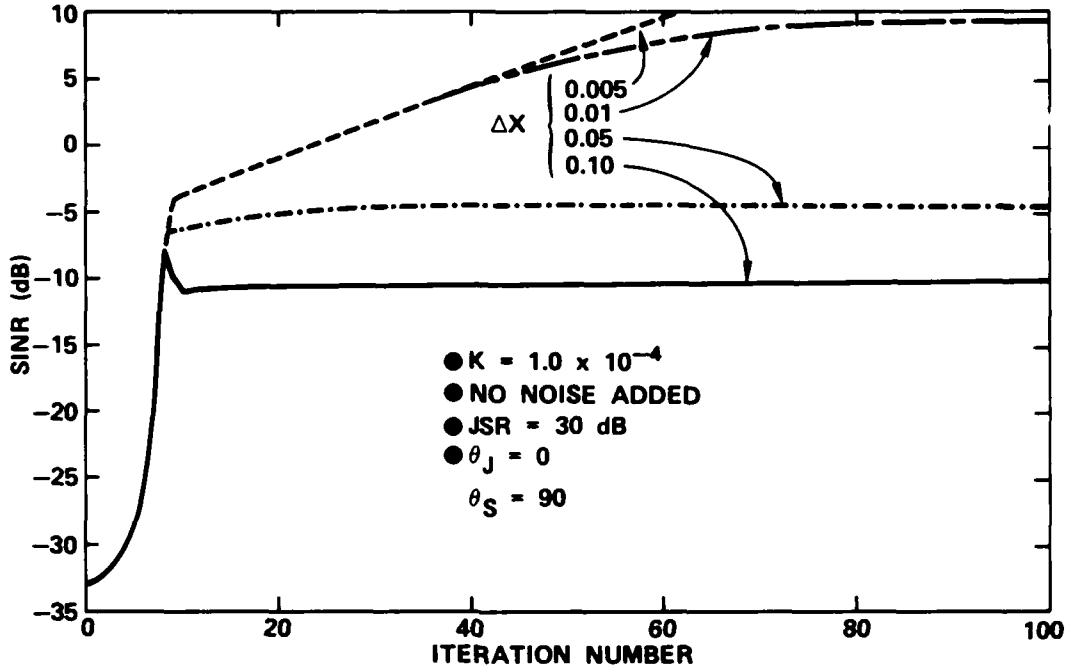

FIGURE 5. Transient Response with ΔX as a Parameter for DS Mode Control.

In Figure 6 we show the transient response for the PI mode for a single broadside jammer with K as a parameter. The behavior of the curves in Figure 6 is similar to the behavior described in Reference 12 and to the behavior of all adaptive arrays controlled by gradient algorithms: the smaller the value of K, the slower is the convergence, but a value that is too large, such as K = 0.0007, can be unstable. For the array configuration of Figure 6, a value of K = 0.0003 appears to be a good compromise. Figure 7 is a plot of the transient response for a RESAA operating in a DS mode, with a desired signal at endfire incidence. In this case, the numerical value of K for best performance is 0.00015, which is somewhat lower. The PI and DS modes are consistent with each other in rejecting the jammer: both give a rejection of about 45 dB.

TABLE 2. Summary of Figures and Data Presented. Entries in the table are figure numbers showing items in left-hand column.

Number of elements	3	5	7	9
Transient response	5,6,7	26,27		
Antenna patterns	8,9,14,20	22,24,25	31	32,33,34
Jammer power vs spacing	10,15	21		
SJR vs spacing		23	30	
Control surface	12,17			
Frequency response	11	29		

THREE-ELEMENT ARRAY

Broadside Jammer

Transient Response. A detailed investigation of the transient response is important to determine preferred values for K and ΔX and to determine the effect of receiver noise on RESAA performance. A best value for ΔX was selected on the basis of transient response curves similar to Figure 5. These curves show that a value of ΔX = 0.5 ohm is sufficiently small to ensure that the control surface gradient is adequately measured for the noise-free case. Values larger than 0.5 ohm are too coarse and cannot measure the gradient at the minimum.

If receiver noise is not included in the simulation, the smallest possible value of ΔX is determined by computer round-off errors. In an actual system, however, the lower bound on ΔX is established by receiver noise. If ΔX were too small, fluctuations in receiver output due to noise would be incorrectly interpreted as changes in the control function that guides convergence. We made a series of runs in which receiver noise was simulated by a Gaussian random number generating routine. For reasonable signal-to-noise ratios (20 dB), a value of ΔX = 0.5 ohm was found to be a good compromise between overly coarse gradient measurement and susceptibility to receiver noise over a very wide range of conditions. We used this value of ΔX in all of the simulations described below.

SIMULATION RESULTS

ASSUMPTIONS, CONVENTIONS, AND ORDER OF PRESENTATION

For convenience, the assumptions and conventions we have adopted for these simulations are listed here.

- The radius of the dipole is 0.01λ.
- The array patterns are normalized to the output that a single dipole element of half-height $H = 0.25\lambda$ would produce.
- In the PI mode, all jammers are assumed to have a power of 1000, and the RESAA output is expressed as a "null depth" relative to this 30 dB jammer.
- In the DS mode, all jammers are assumed to have a power of 1000 relative to an incident signal power of unity. That is, the SJR for each jammer is -30 dB. In some cases, we plot the total jammer power; in others, we plot the SJR.
- The term "pattern null" is used to refer to a minimum in the array pattern that is at least 30 dB below the dipole reference level.
- Each run was stopped after 300 iterations, unless otherwise stated.
- Except for several runs expressly for the purpose of examining the effect of noise, N_o in Equation 5 was set to zero.

We investigated the array behavior using the algorithms described below. Many sets of jammer incidence angles were examined, but the selection cannot be termed exhaustive. Conceivably, particular combinations of jammer incidence angles exist that result in nulling behavior inconsistent with the findings given below.

Table 2 is a summary of the array configurations and parameters considered in the simulations and serves as a guide to the discussion below.

Existence of Optimum Spacing

A RESAA clearly has a spacing that is "optimum" in some sense of the word. For large spacings, the mutual coupling between the elements is small so that the pattern-forming ability is nonexistent; as the spacing is made smaller, the total RF phase shift across the array aperture decreases so that at some point the pattern-forming ability is adversely affected.

To determine the best spacing, the nulling behavior was investigated as a function of number of elements, element spacing, and number of jammers. The three-element array was examined in particular detail, because the shape of the control surface can be readily displayed. This allows more understanding to be gained of the nulling behavior as a function of spacing than with the control surfaces of higher dimensionality resulting from arrays with larger number of elements.

Number of Steerable Pattern Nulls

For a conventional (fully driven) array, the number of jammers that can be nulled by an N-element array is (N-1). This result follows directly from the fact that the total output P from such an array can be written as a linear combination of the steering vectors $\vec{U}(\theta_J)$ for each jammer and the weight vector W in the form (Reference 12)

$$P = \vec{W} \cdot (\vec{U}_1 + \vec{U}_2 + \ldots + \vec{U}_M) \tag{11}$$

where, as a shorthand, we have used the notation $\vec{U}(\theta_{Jm}) = \vec{U}_m$ and where M jammers are present. By the Gram-Schmidt orthogonalization procedure, the components of the N-dimensional vector $\vec{W}$ can be chosen to make $\vec{W}$ orthogonal to no more than (N-1) of the $\vec{U}_m$. Orthogonality implies $\vec{W} \cdot \vec{U} = 0$; hence, (N-1) jammers can be nulled.

Equation 5 expresses the RESAA output comparable to Equation 11 for a conventional array. The nonlinear form of Equation 5 does not permit any procedure akin to Gram-Schmidt orthogonalization to be invoked to determine the number of nullable jammers. One conceivable method to determine the number of nulls is, from Equation 5, to form $\partial P/\partial X = 0$ for $i = 1 \ldots N$ with M jammers, solve the resulting set of N equations for the $(X_L)_{min}$, and then examine the number of minima in $P(\theta)$. However, for even the simplest possible case of two elements, one reactive load, and one jammer, this procedure runs into problems: the equation that results for X_L is fifth order and cannot be solved by other than numerical methods.

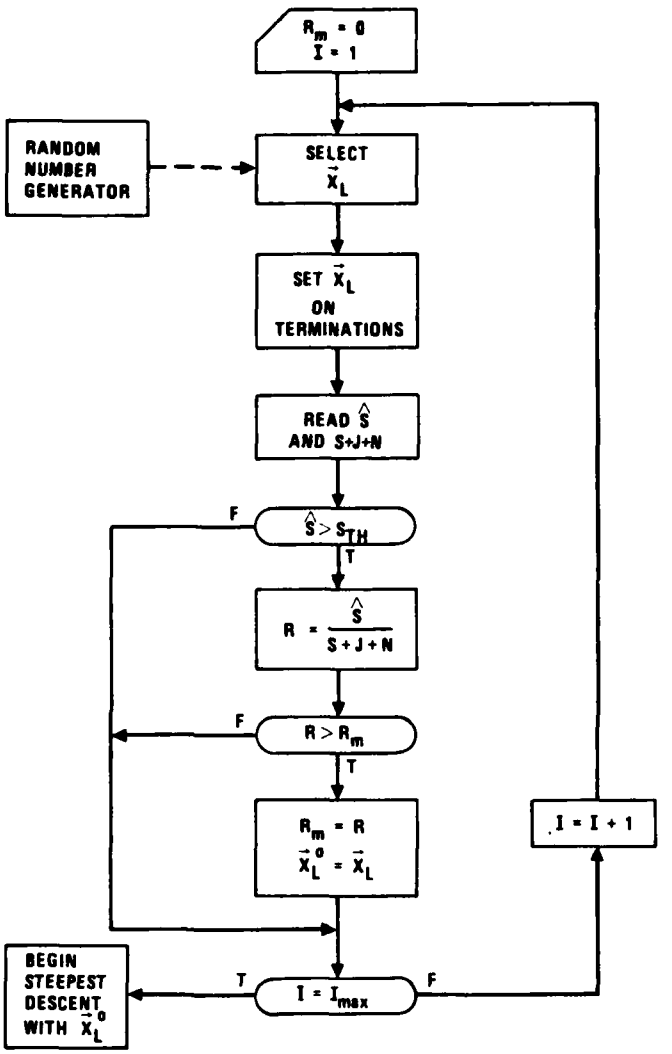

FIGURE 4. Flowchart for Maintaining Antenna Pattern Response in Direction of Desired Signal During Random Search Phase. The quantity $\hat{S}_{th}$ is the minimum allowable response in the desired signal direction, and S is the measured estimate of the desired signal power.

Antenna response towards the desired signal is maintained during the random search and steepest descent phases as follows (cf., Figure 4). During the random search phase, any set of reactive load values that causes the desired signal power estimate to drop below a preset value is rejected as a possible starting point for the subsequent steepest descent processing.* During the steepest descent or optimum gradient processing, the estimate of the signal power is used to form SJR, and (1/SJR) is then used as the criterion function in Equation (8).

The DS mode is particularily necessary when more than one jammer is present to avoid an adapted pattern that places a null towards a desired signal. For a single jammer, the adapted patterns tend to be omnidirectional at incidence angles removed from the jammer angle, so that accidental nulls towards the desired signal are not a problem.

* If the jammer power is high enough and/or desired signal power is low enough to deny any estimate of desired signal strength (which implies that the SJR is less than the null-depth-to-pattern-peak ratio attainable during the random search phase), then a power inversion algorithm can initially be used to improve the SJR without fear of simultaneously nulling the desired signal. Of course, there is still the chance of placing an "accidental" null in the pattern towards a desired signal during this power inversion phase, because the receiver has no knowledge of the desired signal.

This method finds the minimum value of the surface in the fewest possible number of steps, where "step" is defined as each change in the direction of the gradient. However, a large number of intermediate computer calculations are required during each step to find K'. Reference 10 suggests a binary step method for finding K' that might make the optimum gradient technique useful for control of a hardware array. For the present study, however, we determined K' at each step by proceeding along the direction of $\nabla\varepsilon$ in 0.5 ohm increments until the sought-for minimum in ε was found.

Figure 3 also displays the path followed by the optimum gradient method starting from (-50,-50). As is evident, the optimum gradient method finds the minimum in significantly fewer steps. For the calculations in this report, we used the optimum gradient method primarily as a check on the solution points found by the steepest descent method.

Power Inversion Mode and Desired Signal Mode

Two distinct modes of operation are considered in the simulations. The power inversion (PI) mode assumes that no desired signal is incident on the array; the algorithms operate on all incident signals. The criterion function for the PI mode is simply the receiver output, and the algorithms attempt to form the antenna pattern to minimize the total receiver power. The term "power inversion" refers to the fact that usually the adapted receiver output is inversely proportional to its contribution to the total incident jammer power.*

The other mode used in the simulations assumes a desired signal is incident on the array, thus requiring a reasonable antenna pattern response to be maintained in its direction. We refer to this mode as the desired signal (DS) mode. The technique for maintaining response towards a desired signal is shown in Figure 4. It assumes that an estimate of the desired signal power can be derived, at least when the signal-to-jammer ratio (SJR) is sufficiently large. In an actual system, the signal can be distinguished by frequency (e.g., a narrow band filter) or time (e.g., pseudo-noise sequence correlation) characteristics. In the simulations, we are not concerned with the details of deriving an estimate of the signal power; we assume the existence of this estimate.

* This is not always the case with the RESAA because of the nonlinear dependence of the array output on the controlled variables and because of the existence of suboptimal minima in the control surface. We still use the term power inversion, however.

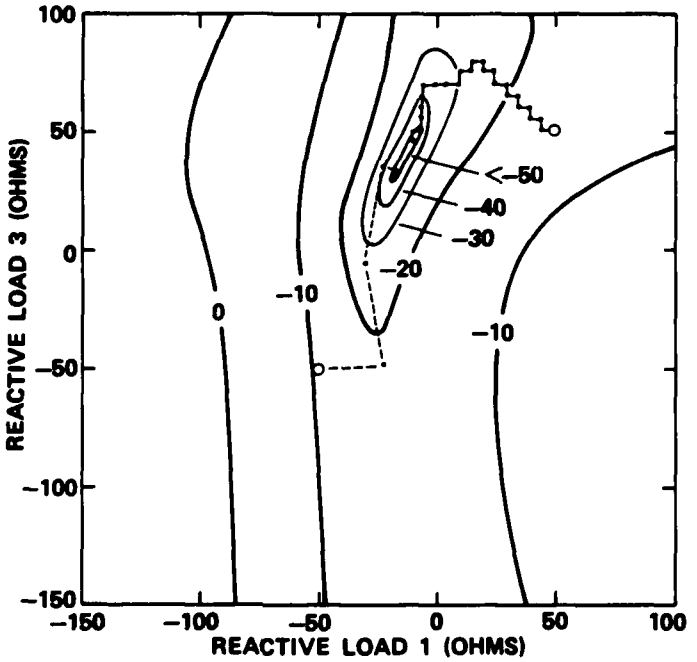

FIGURE 3. Control Surface Contours Showing Two Paths of Convergence. Dashed convergence curve is path for control by optimum gradient method, and solid convergence curve is path for control by steepest descent method. Contours are in decibels relative to dipole antenna response.

Optimum Gradient

The optimum gradient method (Reference 9) can be viewed as a steepest descent technique with a variable value of K. At each point of the process the new direction is computed as $\nabla\varepsilon$, as before, but the value of K in Equation 8 is selected in such a way that the resulting step leads to the minimum possible value of ε along the gradient direction. That is, the best value of K, denoted K', is obtained from

$$\min_{K>0}\left[\varepsilon(X_L(j)-K\nabla\varepsilon)\right] \equiv \varepsilon(\vec{X}(j)-K'\nabla\varepsilon) \tag{9}$$

The new value of the reactive load vector then becomes

$$\vec{X}_L(j+1) = \vec{X}_L(j) - K'\nabla\varepsilon \tag{10}$$

signal, ε was the total jammer power; for null steering with a desired signal, ε was 1/(SJR).*

In Reference 2 $\nabla\varepsilon$ was estimated for the experimental array by sequential variation (Reference 9): only one component of the gradient was measured at a time. If that measurement produced a decrease in ε, then the value of X_{Li} was immediately changed, rather than waiting for a simultaneous change in all reactive loads after all components of $\nabla\varepsilon$ had been measured. For the results below, this procedure was not followed; instead, at each point the gradient was calculated using $\nabla\varepsilon = \nabla\varepsilon/\Delta X$, and then all reactive loads changed according to Equation 8 to obtain the next point.

Figure 3 shows an example of the path followed by steepest descent. A contour plot for a three-element array is shown, along with a path from the initial point (50,50) to the minimum at (-12,48).

* The units of K depend on the criterion function and on the units for X, and have the form (X units)^2/(criterion units). For X in ohms and ε in watts, for example, the units are ohm^2/watt. However, all of the simulations used a reactance normalized to 50 ohms and powers in dB normalized as mentioned earlier. Hence, K is unitless and thus we show no units for K in the results below.

efficient hardware/software implementation. On the other hand, the Rosenbrock algorithm (Reference 10), used by Harrington in a gain optimization study of reactively loaded arrays (Reference 11), is a superior computer code for optimization, but is probably unsuitable for practical control of an array because of the number of computations needed at each step.

For the present study, we used search algorithms that operated as closely as possible to algorithms that are practical for a hardware array. In some cases, particularly for arrays with a large number of elements (i.e., nine or greater), methods exist that could find a control point (that is, a set of reactive loads to perform the desired task, such as nulling multiple jammers) that could not be found by the simpler methods we have used. However, these other methods are principally of academic interest.

We have used combinations of three techniques: (1) random search, (2) steepest descent, and (3) optimum gradient.

Random Search

Random search was used to select an initial set of reactive loads for subsequent optimization by the other two techniques. Sets of reactive loads selected over the range of -300 to 300 ohms were drawn by a uniform random number generator, and the set producing the best value of the parameter being optimized (total jammer power or SJR) was saved as the starting point. For most of the runs, 300 random samples were used.

Steepest Descent

The method of steepest descent uses the equation

$$\vec{X}_L(j+1) = \vec{X}_L(j) - K\nabla\varepsilon \tag{8}$$

to generate values $X_L(j+1)$ of the reactive load at the $(j+1)$ step from values at the jth step. The quantity K is a positive constant that controls the rate of descent, and $\nabla\varepsilon$ is the gradient vector of the criterion function ε. The criterion function depended on the particular problem. For steering nulls on jammers with no desired

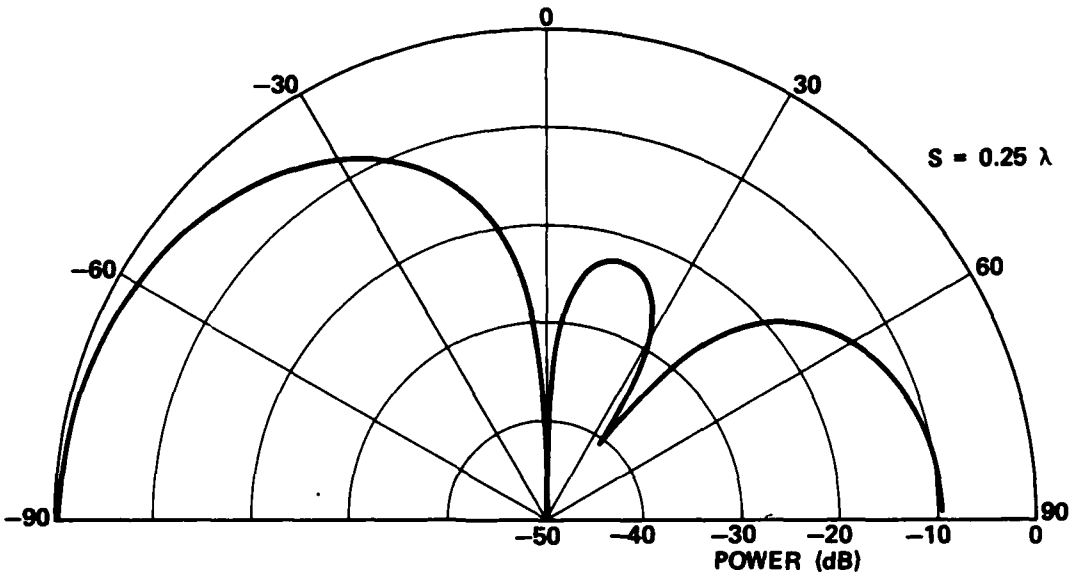

(d) Spacing = 0.25λ.

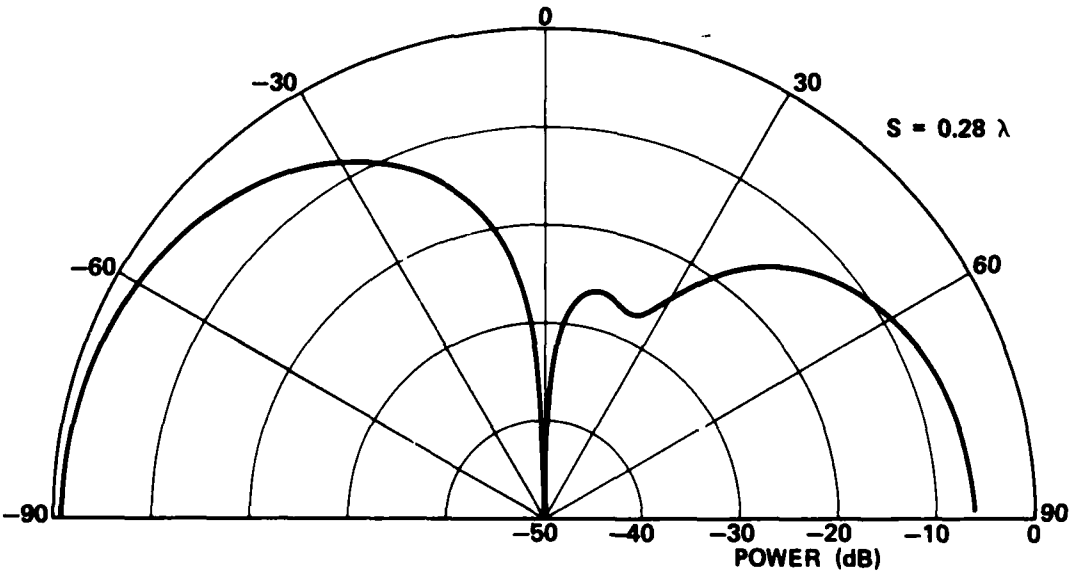

(e) Spacing = 0.28λ.

FIGURE 9. (Contd.)

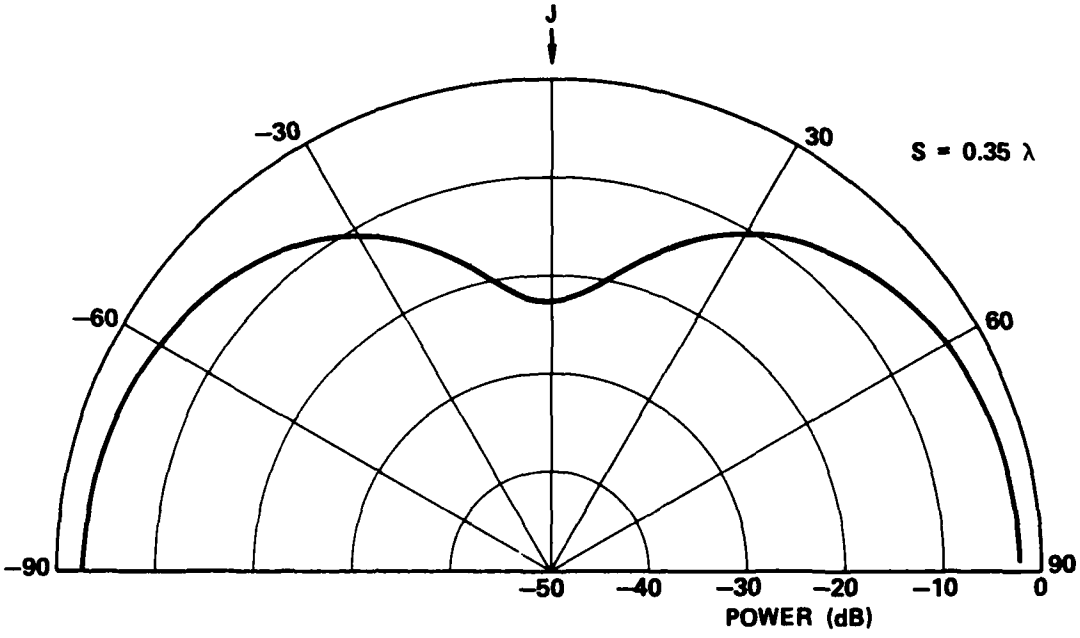

(f) Spacing = 0.35λ.

FIGURE 9. (Contd.)

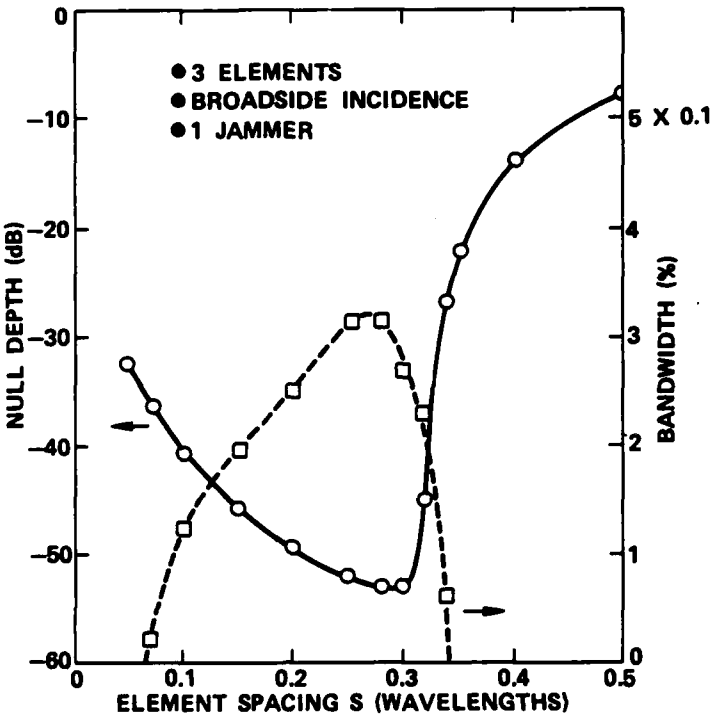

FIGURE 10. Null Depth and Nulling Bandwidth for Three-Element Array for Jammer Incident at 0 Degrees.

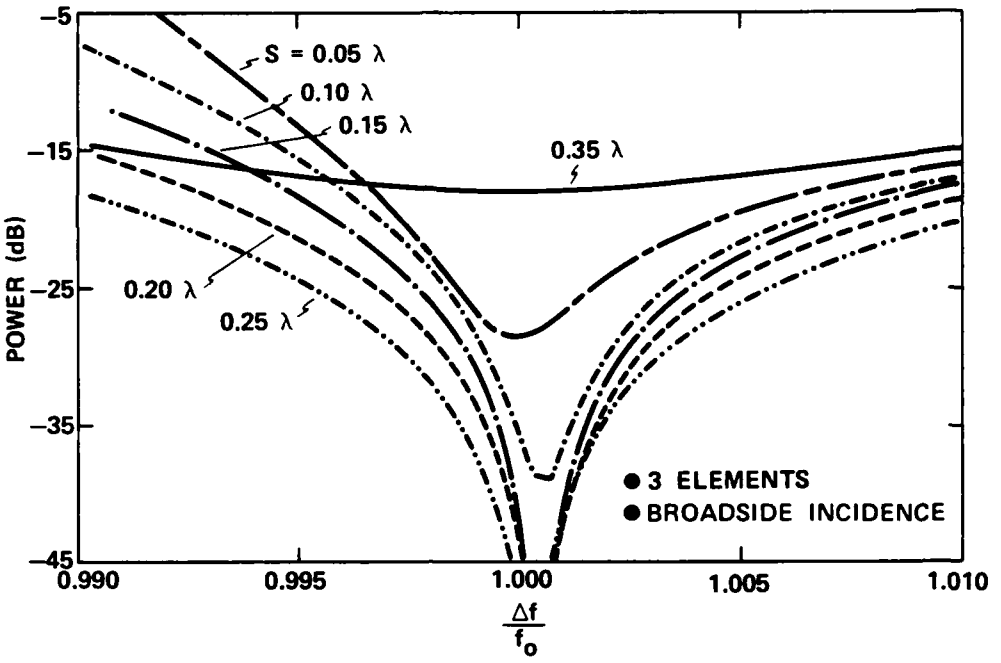

FIGURE 11. Null Frequency Response.

As is evident from Figures 9 through 11, the range of spacings from about 0.15 to 0.30λ produces nulls that are deeper and have a broader bandwidth than smaller or greater spacings. On the basis of these curves, any spacing within this range can be considered optimum. Of particular interest is the sharp degradation in null depth as the spacing is made greater than 0.32λ. An understanding of what happens near S = 0.32λ can be gained from the control surfaces in Figure 12. In Figure 13 the loci of the minima in Figure 12 are plotted. For a spacing less than about 0.32λ, there are two minima in the control surface, but, at S = 0.32λ, these minima coalesce into a single shallow minimum that persists for S > 0.32λ. The onset of the shallow null coincides with the coalescence of the two minima.

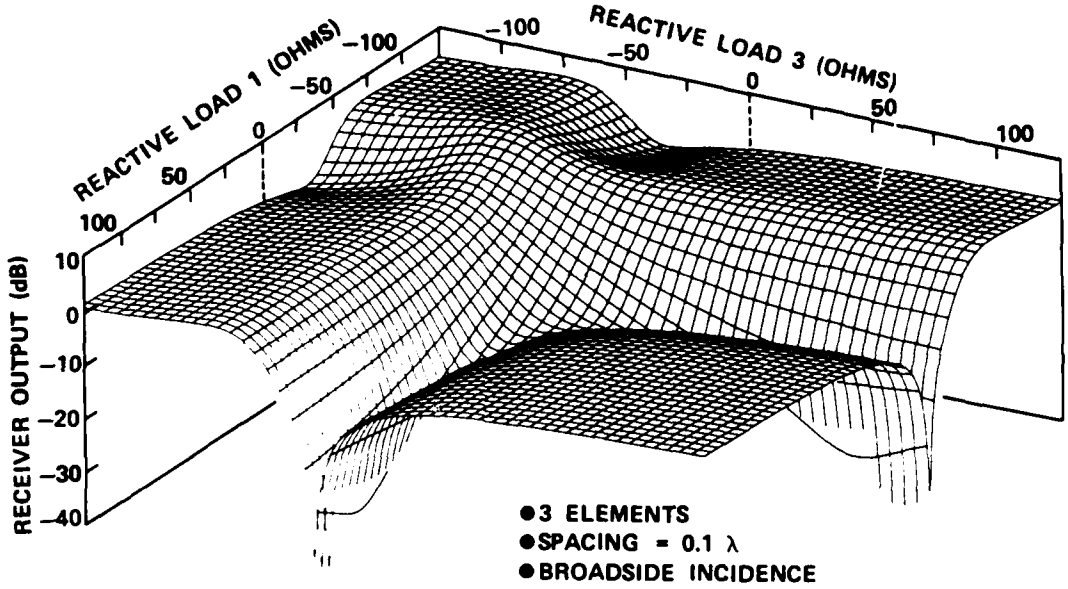

(a) Spacing = 0.1λ.

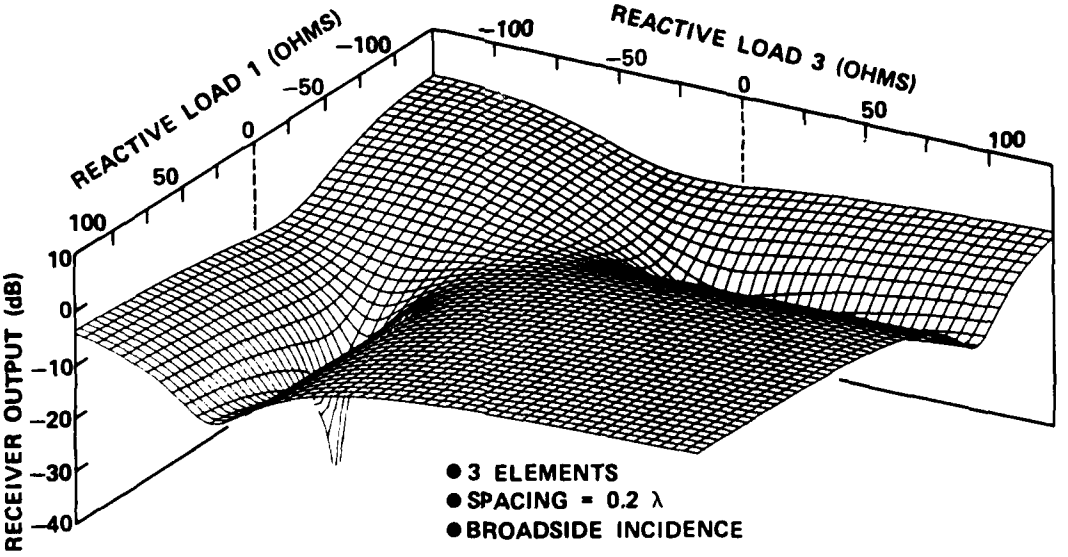

(b) Spacing = 0.2λ.

FIGURE 12. Control Surface for Three-Element Array. The vertical axis on each plot is the receiver output as a function of the reactive load on elements 1 and 3.

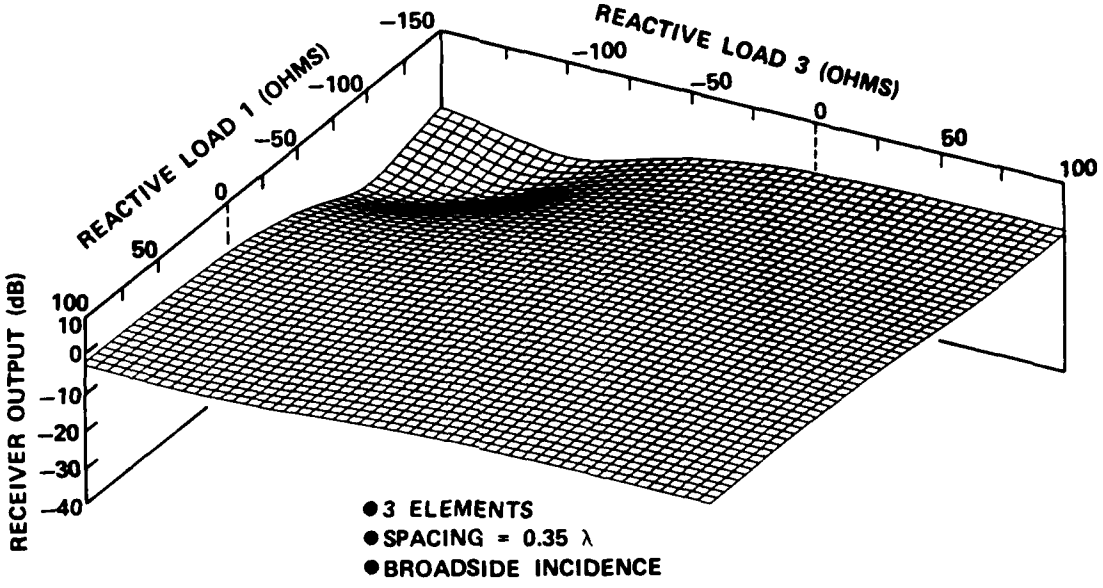

(c) Spacing = 0.35λ.

FIGURE 12. (Contd.)

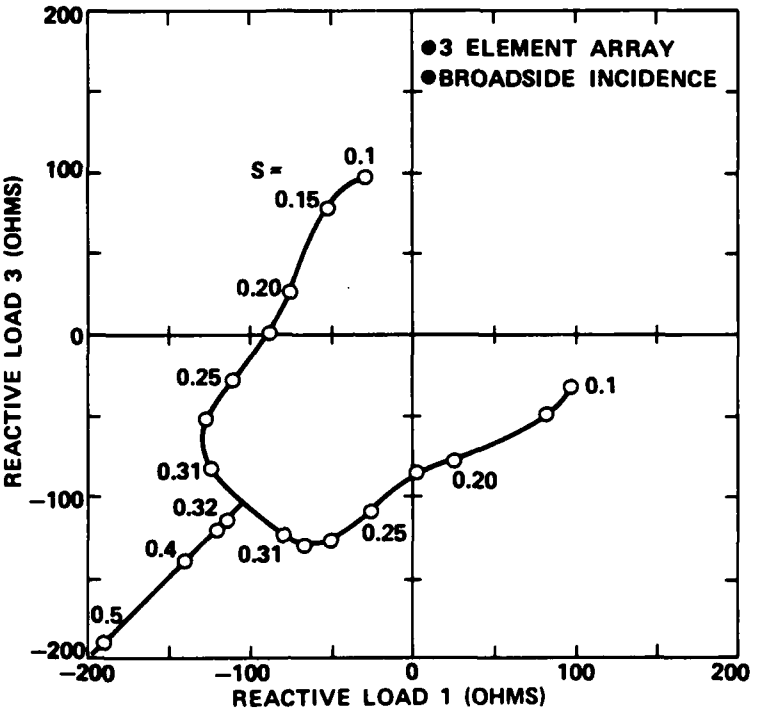

FIGURE 13. Loci of the Minima in the Control Surface for a Three-Element Array and a Broadside Jammer. Spacing in wavelengths shown at various points along the curve.

Endfire Jammer

Figure 14 shows antenna patterns for nulling of an endfire jammer for three different spacings, and Figure 15 plots the null depth and bandwidth as a function of spacing. The behavior for endfire incidence is similar to the behavior for broadside incidence, except that the optimum spacings are substantially smaller. The best spacing is approximately $S = 0.1\lambda$, and spacings greater than 0.2λ produce a poor null.

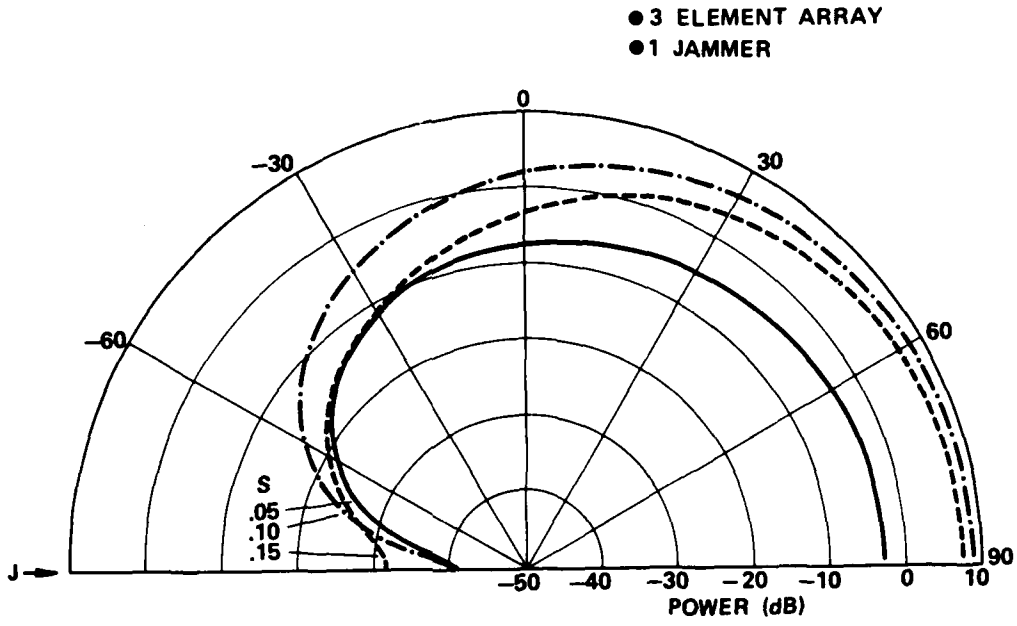

FIGURE 14. Antenna Patterns for Nulling of Jammer at -90 Degrees for Three Different Element Spacings.

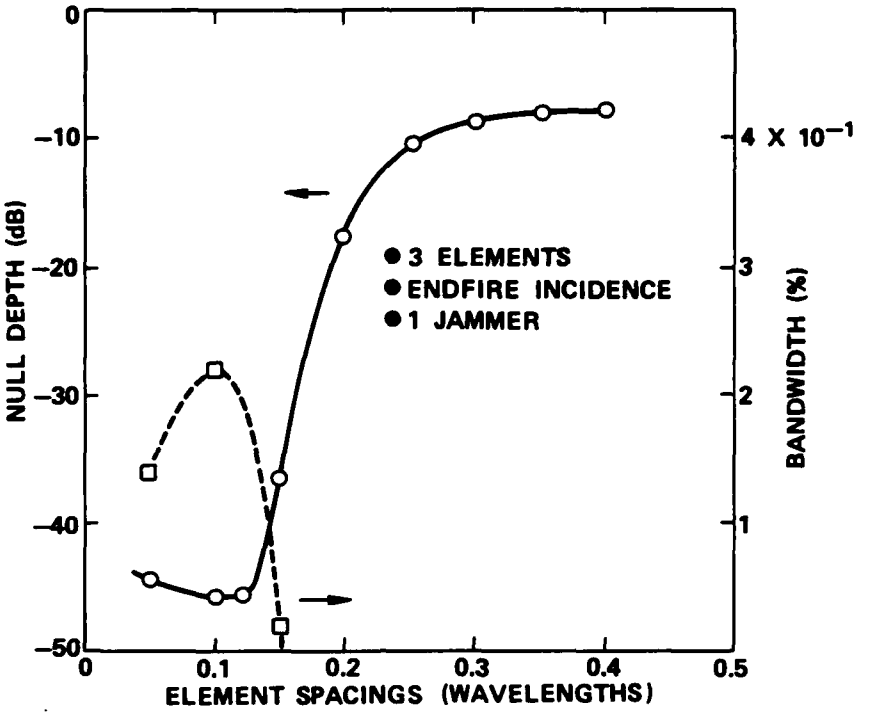

FIGURE 15. Null Depth and Nulling Bandwidth for Three-Element Array for Jammer Incident at 90 Degrees.

As with a broadside jammer, the degradation of the null near S = 0.2λ is associated with the coalescence of two nulls in the control surface. Figure 16 is a plot of the loci of the control surface minima, showing that for S > 0.17λ only a single minimum exists. Figure 17 displays an example of a control surface for endfire incidence.

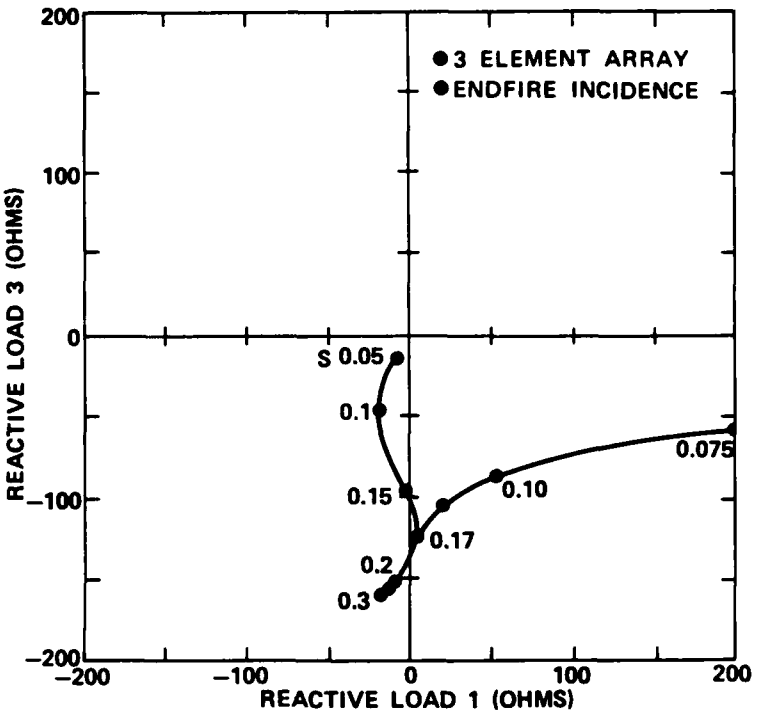

FIGURE 16. Loci of the Minima in the Control Surface for a Three-Element Array and a Jammer Incident at 90 Degrees. Spacing in wavelengths shown at various points along the curve.

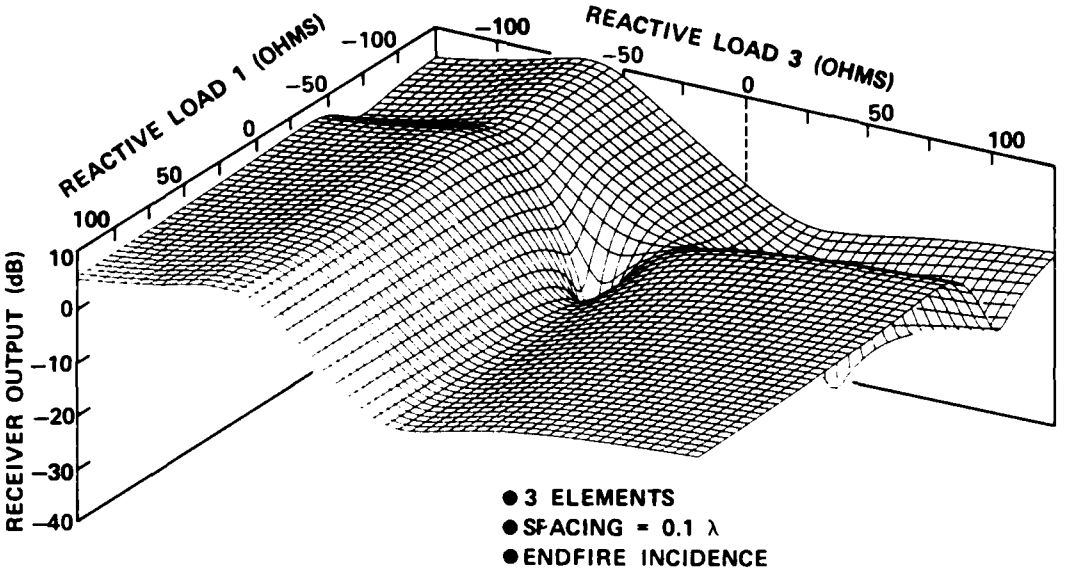

FIGURE 17. Sample Control Surface for Three-Element Array and Jammer Incident at 90 Degrees.

Jammers Incident Between Broadside and Endfire

The pattern observed for broadside and endfire incidence is also followed between these two extremes. In Figure 18 we plot the spacing at which the two nulls coalesce as a function of jammer angle of incidence; as found at $\theta = 0$ degrees and $\theta = 90$ degrees, this spacing is also an upper limit for best nulling.

The conclusions from these results are that a spacing between $S = 0.1\lambda$ and $S = 0.15\lambda$ provides the best performance if a jammer must be nulled at all possible incidence angles; when nulling of a jammer incident only from near broadside is required, a spacing of about 0.25λ is preferred for its wider nulling bandwidth.

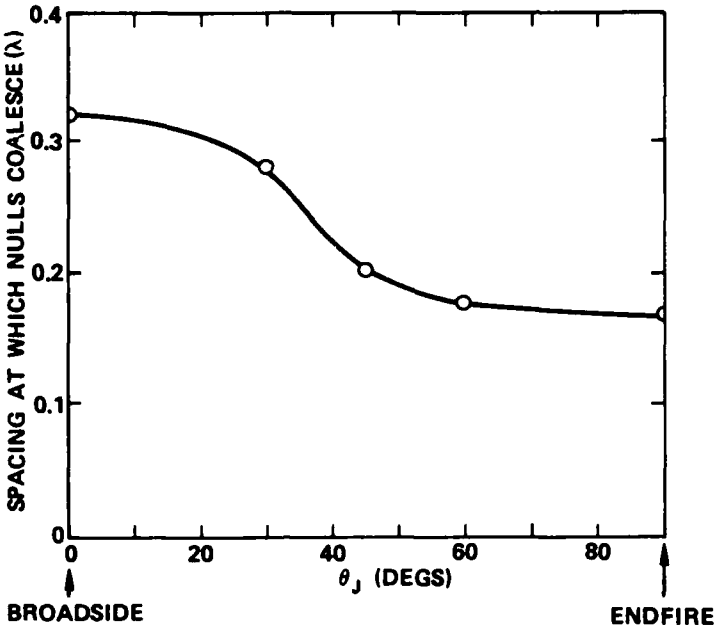

FIGURE 18. Spacing at Which the Two Control Surface Minima Coalesce for a Three-Element Array as a Function of Jammer Angle of Incidence.

Multiple Jammers

The previous sections demonstrated that a single jammer could be nulled and that a spacing of S =0.1λ guaranteed nulling from any angle of incidence. The prime question then: Can two jammers be nulled?

The answer is no. From repeated trials with two jammers incident on the array from various combinations of angles, we have concluded that two independently steerable nulls cannot be formed. Figure 19 shows an example of nulling attempts on two jammers, where J1 is fixed at θ = 60 degrees and the angle of incidence of J2 is varied between -90 and +90 degrees. The received power of each jammer is plotted as a function of θ_{J2}, the angle of incidence of J2. Except for θ_{J2} = 60 degrees, which is the trivial case where J1 coincides with J2, neither jammer is nulled.

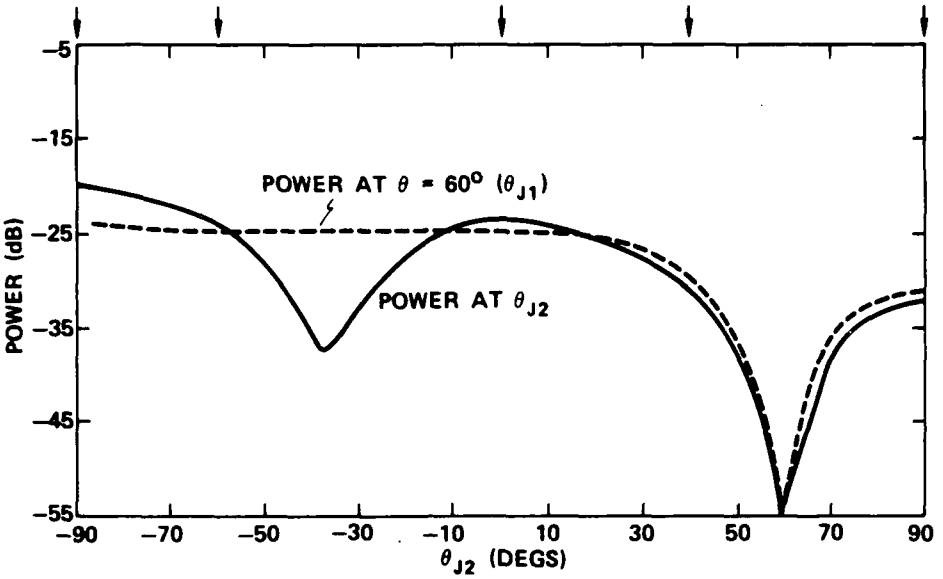

FIGURE 19. Array Pattern Value for Two Jammers Incident on a Three-Element Array. Jammer 1 is fixed at 60 degrees, and jammer 2 is varied in incident angle from -90 to 90 degrees. The arrows along the top of the figure indicate points at which patterns are given in Figure 20.

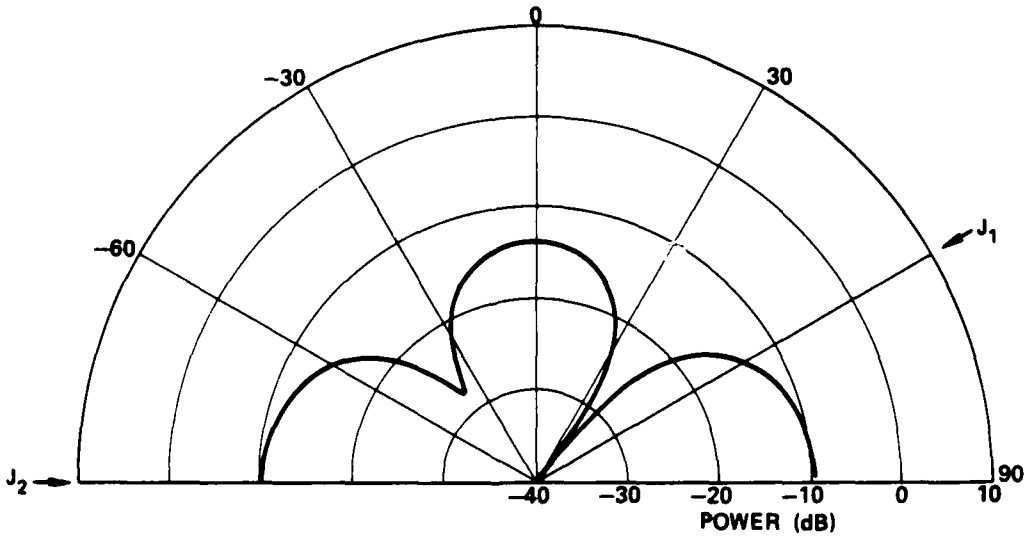

(a) J2 = -90 degrees.

FIGURE 20. Antenna Patterns at Points Indicated in Figure 19.

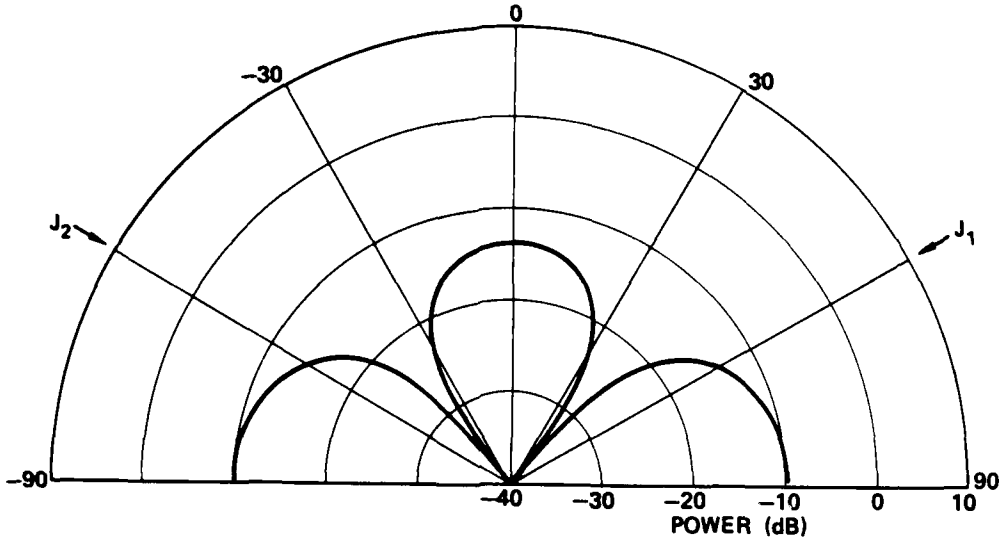

(b) J2 = -60 degrees.

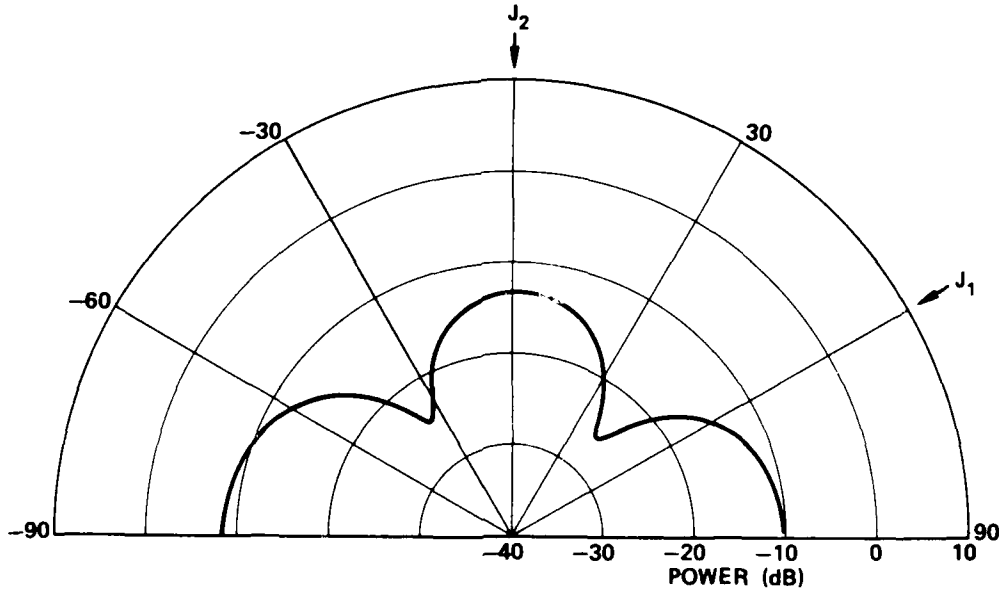

(c) J2 = 0 degrees.

FIGURE 20. (Contd.)

As was done for the five-element array, we conducted a series of runs to determine the manner in which the SJR varied as θ_S was made to approach θ_J. The behavior was similar to the behavior plotted in Figure 28 for the five-element array.

Given the generally favorable behavior of the seven-element array operating against three jammers in a DS mode, it is of interest to speculate why the PI mode fails so miserably. The erratic behavior is probably a matter of whether or not the initial point for the steepest descent processing (arrived at by the initial random search phase) falls within a portion of the control surface that permits convergence to the set of reactive loads that is a global optimum. An increased number of random searches, of course, increases the probability of finding a favorable initial point; however, the adaptation time becomes correspondingly longer. We believe the 300 random search steps is as many as is practical. Given this observation, then, the question is: Why does the DS mode not show a similar erratic behavior? Our hypothesis is that the control surface for 1/SJR (the criterion function for the DS mode) has fewer local suboptimal minima, so that the probability of convergence to an acceptable solution is higher.

NINE-ELEMENT ARRAY

The trend in the number of jammers that can be nulled as the number of elements is increased suggests that a nine-element array can null four jammers; however, the experience with the seven-element array (whereby some combinations of three jammers were difficult to null, and only the DS mode was successful) suggests that this trend may not extend to nine elements.

In fact, we found that the trend did not continue: in general, four jammers could not be nulled consistently by a nine-element array. Figure 32 shows a pattern after an attempt to null four jammers and a desired signal that is tantalizingly close to having four pattern nulls towards the jammers; however, the pattern values at -40 and -80 degrees are only about -25 dB. Figure 33 is a more typical pattern after adaptation to four jammers and a desired signal. Only one of the pattern minima actually points directly at a jammer. In general, the DS mode produced erratic results against four jammers, and the PI mode failed completely.

A behavior noted with three jammers against the seven-element array was an occasional run where a large number of iterations were required to obtain nulling (at a value of S within the optimum region of Figure 30). Sometimes, going back in such a run and increasing the number of initial random searches succeeded in decreasing the number of subsequent steepest descent iterations, implying that the random search phase encountered a better set of initial loads. At other times, an increased number of random searches produced no decrease in steepest descent iterations. Our general conclusion is that the control surface for three jammers against a seven-element RESAA can have a large number of suboptimal minima.

In Figure 31 an adapted pattern is shown for case 1 of Table 4. Three minima in the pattern are steered towards the jammers, but the minimum towards the jammer at -20 degrees is not as deep as the other two. In general, we found that one of the minima for three jammers incident on a seven-element array was usually somewhat shallower than the other two. In addition, an additional null has appeared at an angle of 35 degrees. The appearance of such nulls is not usually a problem in a DS mode.

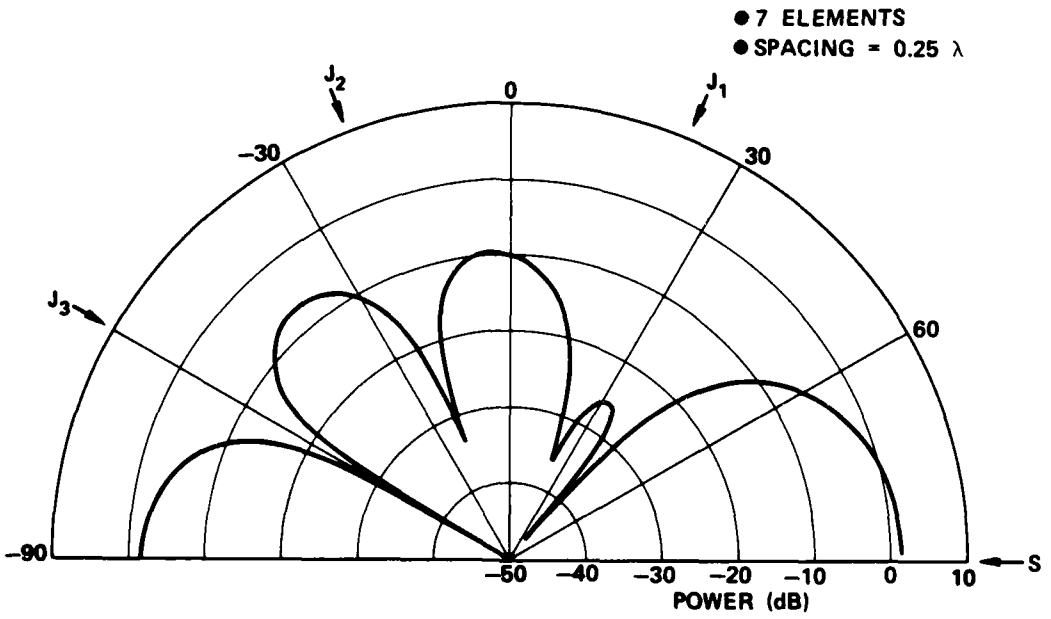

FIGURE 31. Adapted Antenna Pattern for Case 1 of Table 4 at an Element Spacing of 0.25λ.

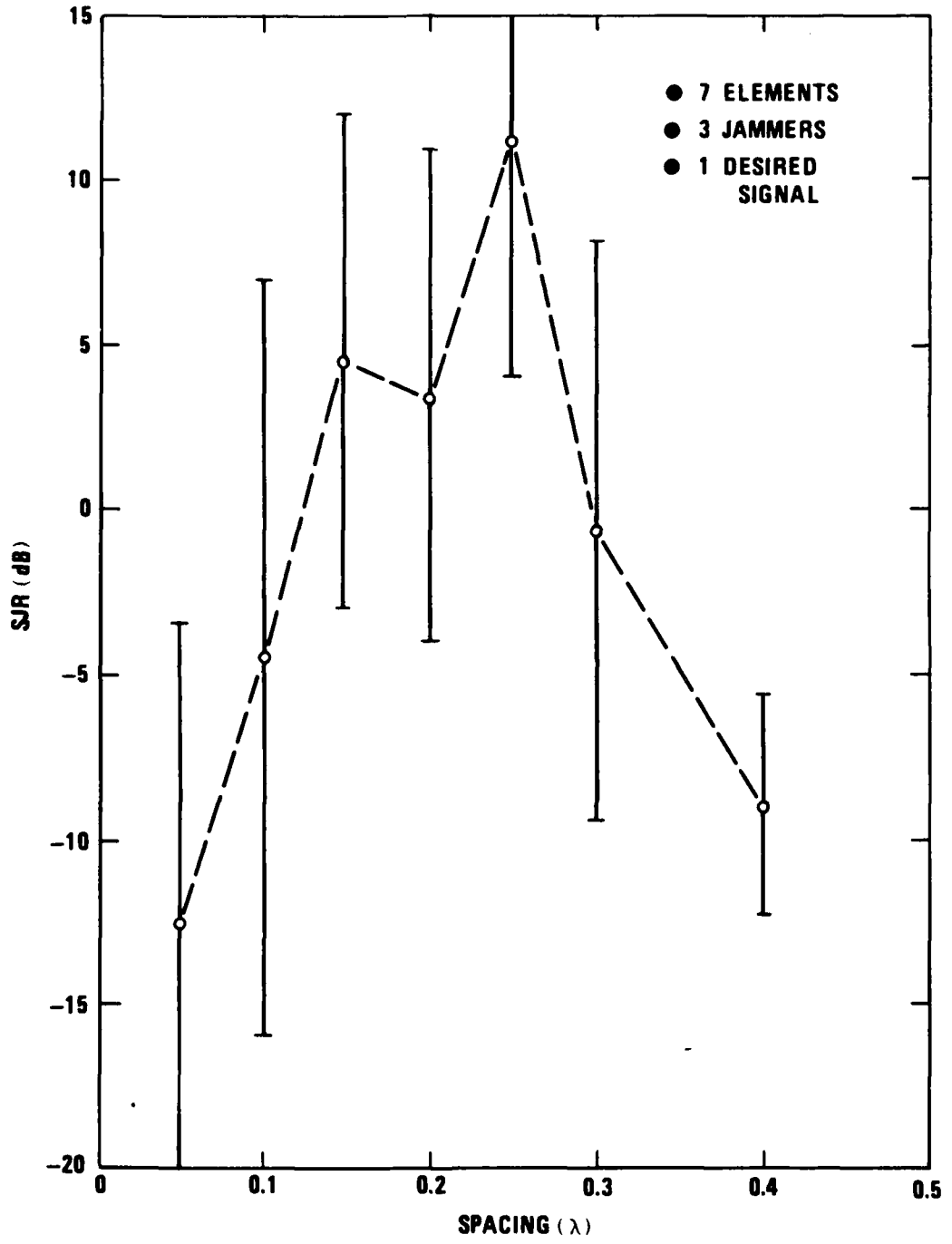

FIGURE 30. SJR Versus Element Spacing for Three Jammers and a Desired Signal Incident on a Seven-Element Array. The average (open circle) and standard deviation (bar) are shown for the four cases whose parameters are given in Table 4.

spacings, and algorithm parameters (ΔX and K) failed to find a combination that would consistently null three jammers. Hence, we only present results for the seven-element RESAA operating in the DS mode.

Figure 30 is a plot of the SJR as a function of the element spacing for three jammers and one desired signal. The results of four runs with varying incidence angles have been averaged for this plot. Table 4 summarizes the parameters for these four runs. The trend in the plot and the range of optimum spacings are approximately the same as was previously found for three- and five-element arrays. Other combinations of jammers and desired signal yield similar curves.

TABLE 4. Summary of Cases Analyzed for Seven-Element Arrays.

Case Number	1	2	3	4
J1 angle of incidence (degrees)	20	-60	0	-30
J2 angle of incidence (degrees)	-20	60	45	-70
J3 angle of incidence (degrees)	-60	20	-60	90
Desired signal angle of incidence (degrees)	90	0	90	30
Highest SJR (dB)	1.0	16.4	17.0	18.6
and spacing (λ) yielding that value	0.2	0.25	0.25	0.25

the null frequency response for a five-element array; shown are the responses for a two-jammer case in a DS mode, and a single jammer case in a PI mode. The nulling bandwidth for all three curves is about 0.15%, which is of the same order of magnitude found for the three-element array. Other runs sometimes gave slightly higher nulling bandwidths.

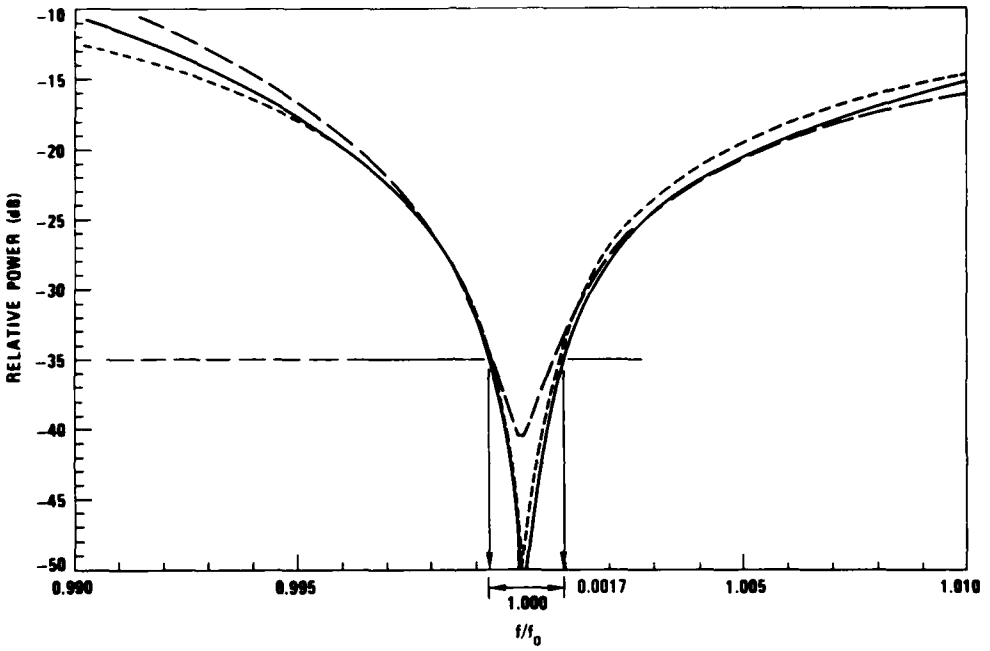

FIGURE 29. Null Frequency Response for Two Cases of Nulling by a Five-Element Array. Case 1: J1 incident at 0 degrees, J2 incident at 60 degrees, desired signal incident at -90 degrees. Solid curve is null frequency response for jammer J1, and dashed curve is null frequency response for jammer J2. Case 2: jammer incident at 60 degrees, no desired signal (PI mode). Dotted curve is frequency response for jammer at 60 degrees.

SEVEN-ELEMENT ARRAY

Extrapolation of the results with three- and five-element arrays suggests that a seven-element array should be able to null three jammers. We found that indeed three jammers could be consistently nulled, but only if the DS mode was used. The PI mode produced erratic results for a seven-element array against three jammers. An extensive series of runs over a large selection of incidence angles,

In Figure 28 we present the results of a series of runs designed to determine the ability of a RESAA to steer a null towards a jammer close in azimuth to the desired signal. Jammers are assumed incident on the array at angles of -90 degrees and 0 degrees, and the desired signal angle is varied. The curve shows that a steady state SJR of 0.0 dB can be achieved as long as the desired signal is no closer than 20 degrees to the jammer. Runs with other sets of jammer angles gave similar results.

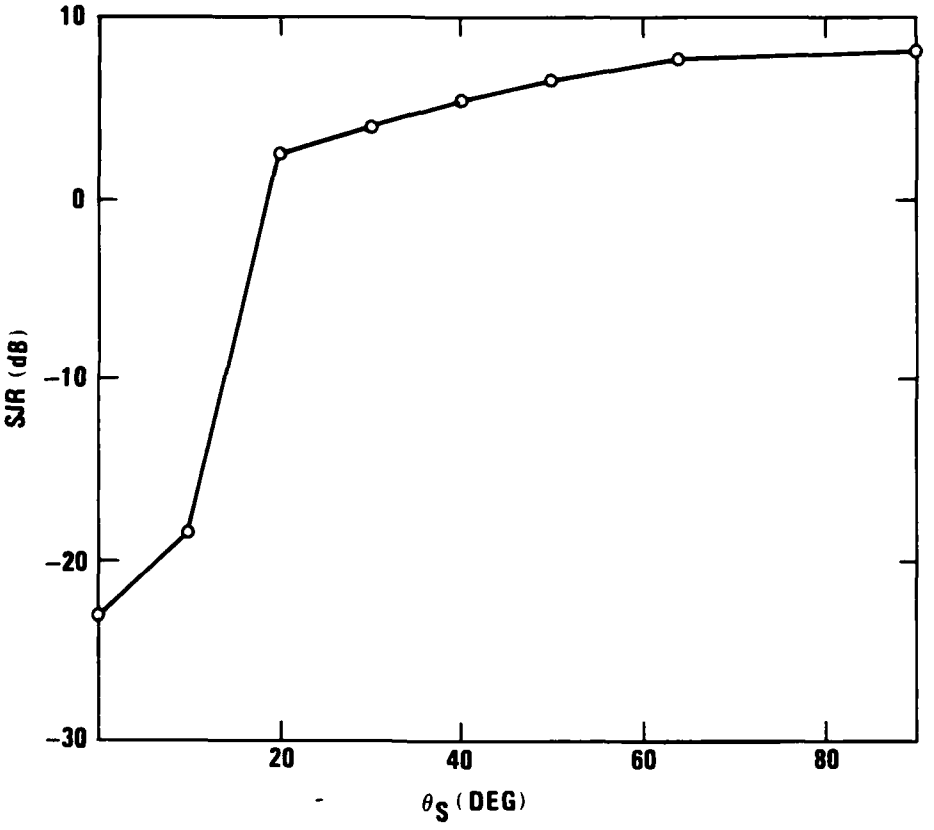

FIGURE 28. Steady State SJR Versus the Angle of Incidence of the Desired Signal for Jammers Fixed at Incidence Angles of -90 and 0 Degrees.

Bandwidth

The behavior of the nulling bandwidth for the five-element array was found to be very similar to the behavior for the three-element array, as were the values of the bandwidth. Figure 29 is a plot of

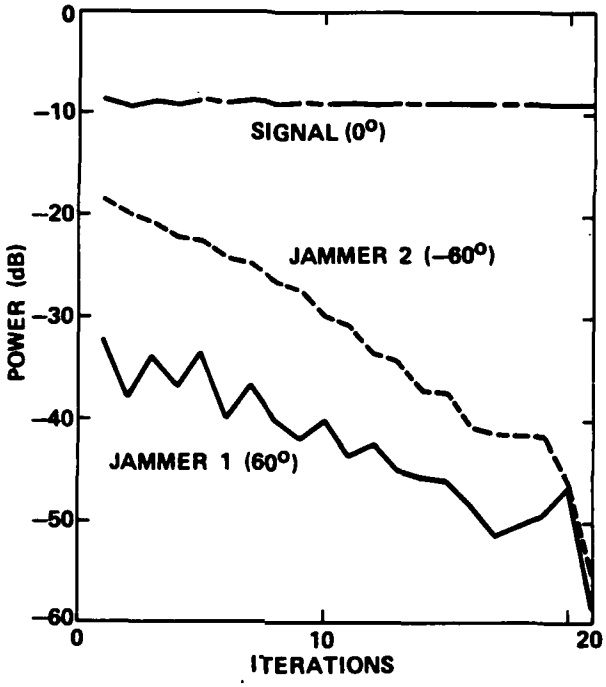

FIGURE 26. Transient Response for Case 1 of Table 3 for Nulling by DS Mode.

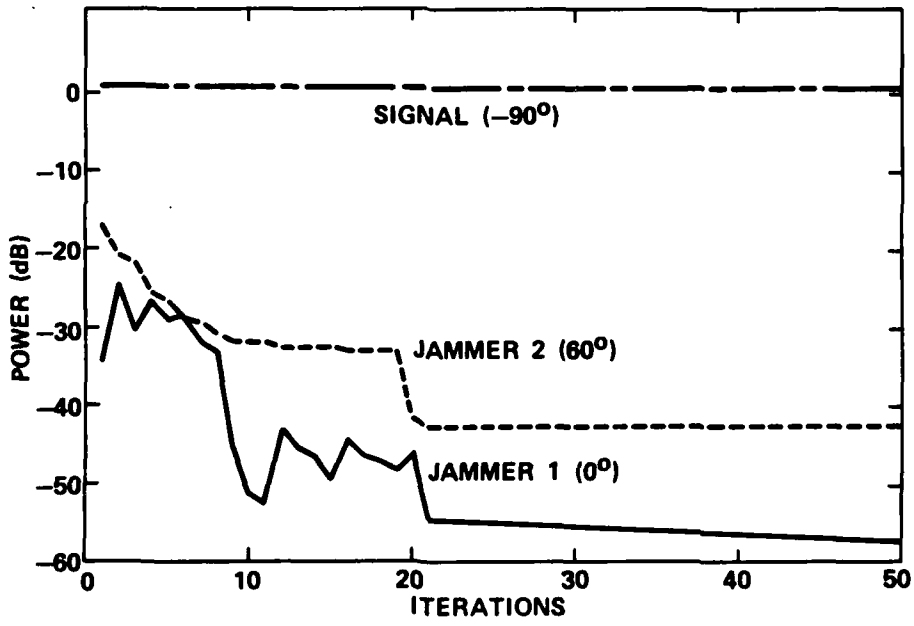

FIGURE 27. Transient Response for Case 3 of Table 3 for Nulling by DS Mode.

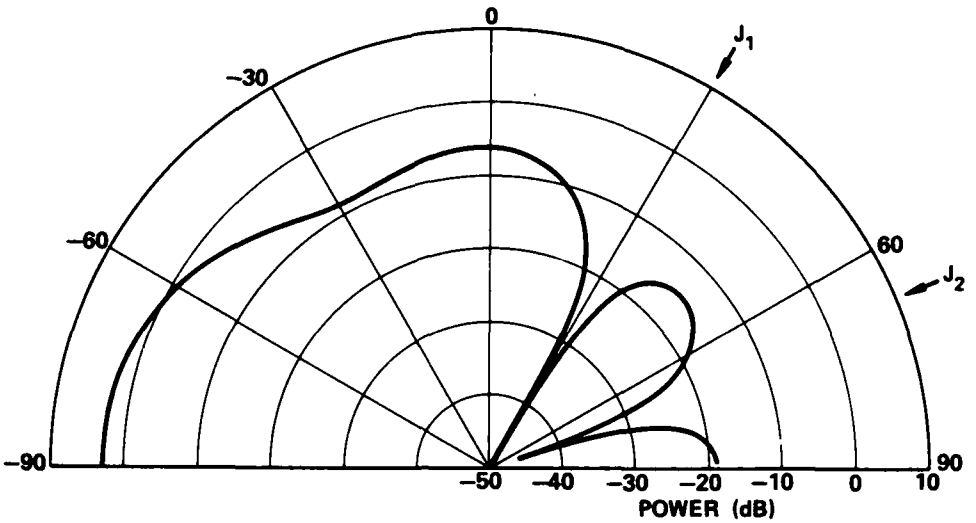

FIGURE 25. Adapted Antenna Pattern for Case 2 of Table 3 at an Element Spacing of 0.2λ.

The transient responses for cases 1 and 3 are shown in Figures 26 and 27, respectively. In each figure the starting values at iteration 1 are the powers at the conclusion of the random search phase. Figure 26 displays the typical transient response: the jammer powers converge more or less monotonically in a smooth fashion to their steady state value after about 20 iterations. Figure 27, on the other hand, is an atypical case. The jammer powers, particularly jammer 1, fluctuate during convergence and then appear to achieve a steady state value at iteration 15 or so. However, at iteration 20 the true minimum in the control surface is arrived at as the jammer powers drop sharply by 10 dB. In both figures the signal power is observed to remain essentially constant.

TABLE 3. Summary of Cases Analyzed for Five-Element Arrays.

Case Number	1	2	3	4
J1 angle of incidence (degrees)	60	30	0	-30
J2 angle of incidence (degrees)	-60	70	60	0
Desired signal angle of incidence (degrees)	0	-90	-90	60
Highest SJR (dB) and element spacing yielding that value (λ)	17.3 0.15	3.65 0.25	2.0 0.1	5.72 0.15

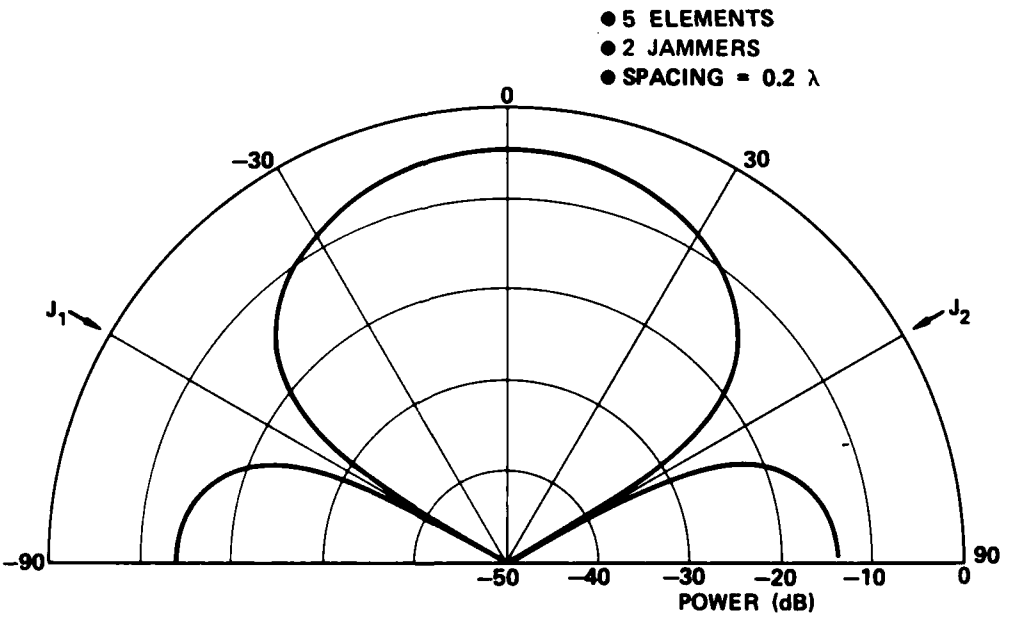

FIGURE 24. Adapted Antenna Pattern for Case 1 of Table 3 at an Element Spacing of 0.2λ.

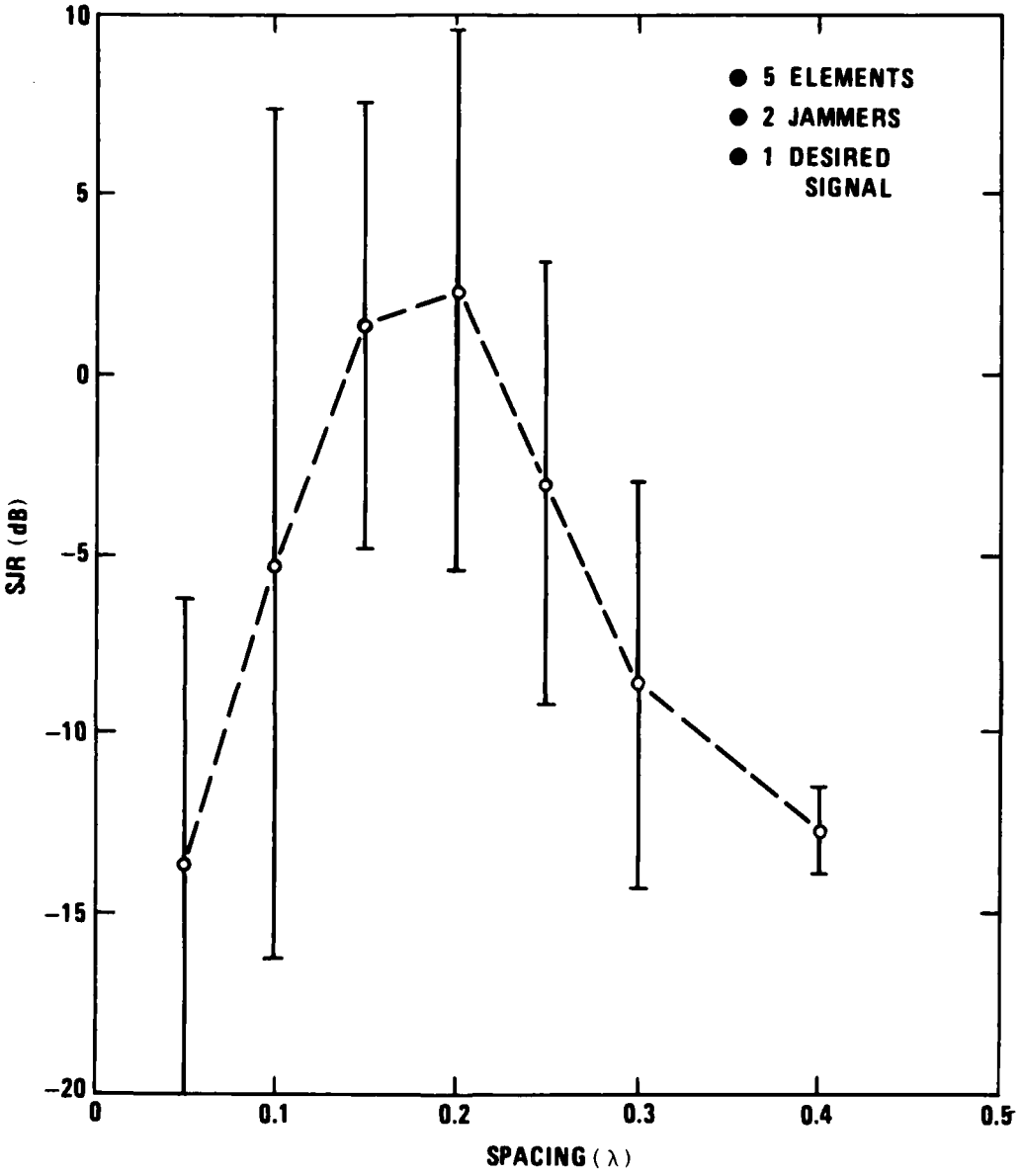

FIGURE 23. SJR Versus Element Spacing for Two Jammers and a Desired Signal Incident on a Five-Element Array. The average (open circle) and standard deviation (bar) are shown for the four cases whose parameters are given in Table 3.

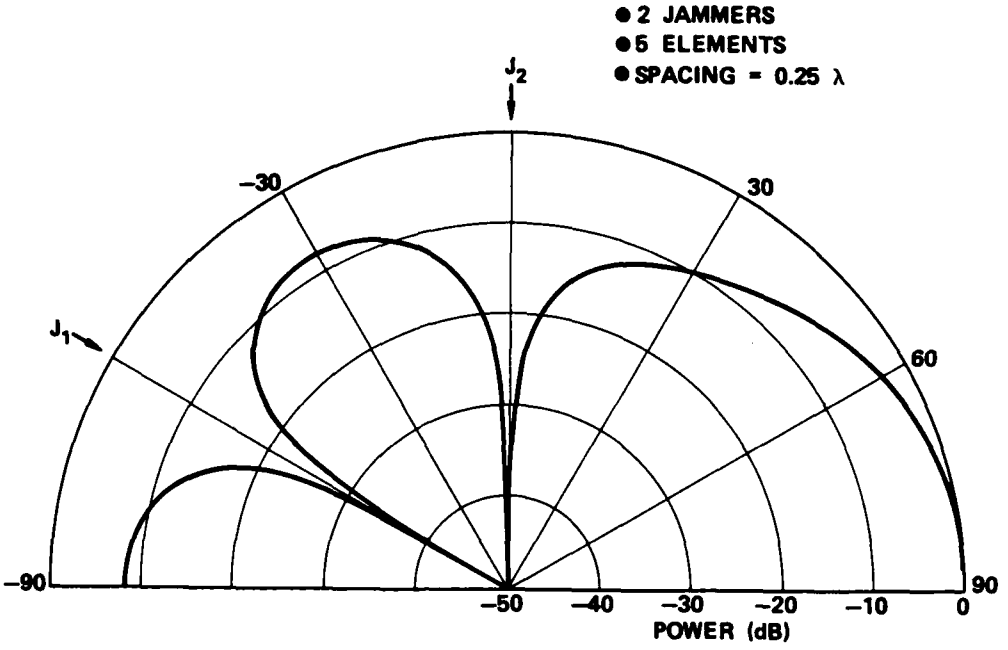

FIGURE 22. Adapted Antenna Pattern for Two Jammers Incident on Five-Element Array. Element Spacing = 0.25λ.

Desired Signal Mode

Figure 23 is a SJR-versus-spacing plot that summarizes the results of four runs with a variety of jammer incidence angles and desired signal angles. In Table 3 we list details of these four cases. The trend of the curve in Figure 23 is similar to the trend already seen in the other performance versus spacing plots: a spacing of about 0.2λ gives the best performance. In Figures 24 and 25 we show adapted antenna patterns for cases 1 and 2 of Table 3.

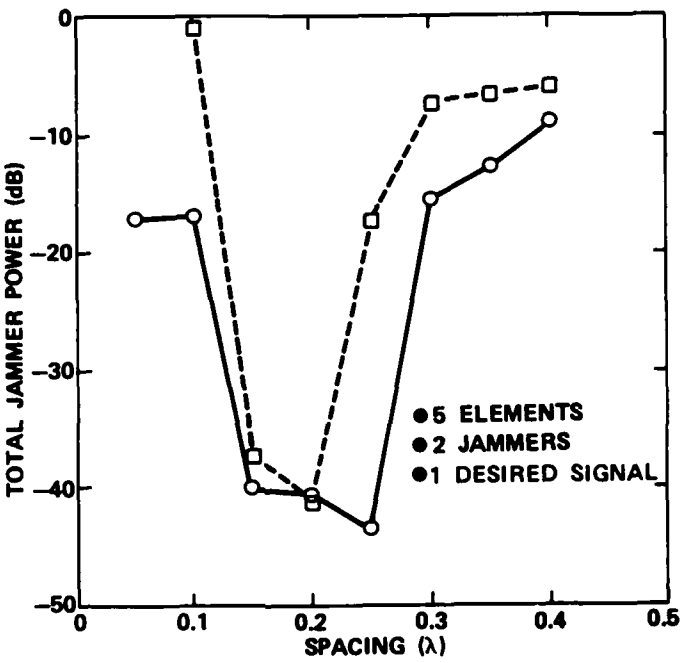

FIGURE 21. Total Jammer Power Appearing at Array Output as a Function of Element Spacing for Two Sets of Jammer Incidence Angles. Dashed curve: θ_{J1} = 60 degrees, θ_{J2} = 20 degrees. Solid curve: θ_{J1} = 0 degrees, θ_{J2} = -60 degrees. Array controlled by PI mode. Five elements.

It is instructive to examine the array antenna patterns. Figure 20 shows the pattern at the points indicated by the arrows in Figure 19. For θ_{J2} greater than about 35 degrees, the adaptive algorithm rotates a single null so as to minimize the total power of the two jammers. For $\theta_{J2} < 35$ degrees, a second minimum appears in the pattern at about $\theta = -40$ degrees; as θ_{J2} decreases further, the position of this minimum remains essentially fixed at -40 degrees and a "mirror image" minimum at $\theta = +40$ degrees forms that also remains fixed. The relative depths of these two minima change according to the combination that minimizes the total power of the two jammer signals, but their azimuth angles of ±40 degrees stay relatively fixed. It is clear that, in general, two nulls cannot be steered with a three-element array.

FIVE-ELEMENT ARRAY

We were able to null two jammers with a five-element array using either the PI mode or the DS mode. Attempts to null three jammers, however, were unsuccessful using either mode. Usually, the pattern would contain only two nulls, neither of which pointed directly towards any of the jammers. Instead, the two nulls adjusted in depth, width, and direction to minimize the performance criterion.

We now discuss the results using two jammers.

Power Inversion Mode

Figure 21 is an example of the variation of total received jammer power for two jammers as a function of element spacing; two curves are shown for two different sets of incidence angles. The shape and trend of these curves are typical of curves for other pairs of jammer angles: the minimum occurs in the vicinity of $S = 0.2\lambda$, and the total jammer power is reduced by about 40 dB.

For all of the pairs of jammer angles investigated (10 pairs of randomly selected values), we were able to form nulls towards both jammers for an element spacing of 0.2λ. Figure 22 gives an example of the antenna pattern for one sample pair of angles. However, the response in other directions sometimes was not always at a level that would be sufficient for receiving a desired signal. Depending on the specific application, a DS mode might be preferable.

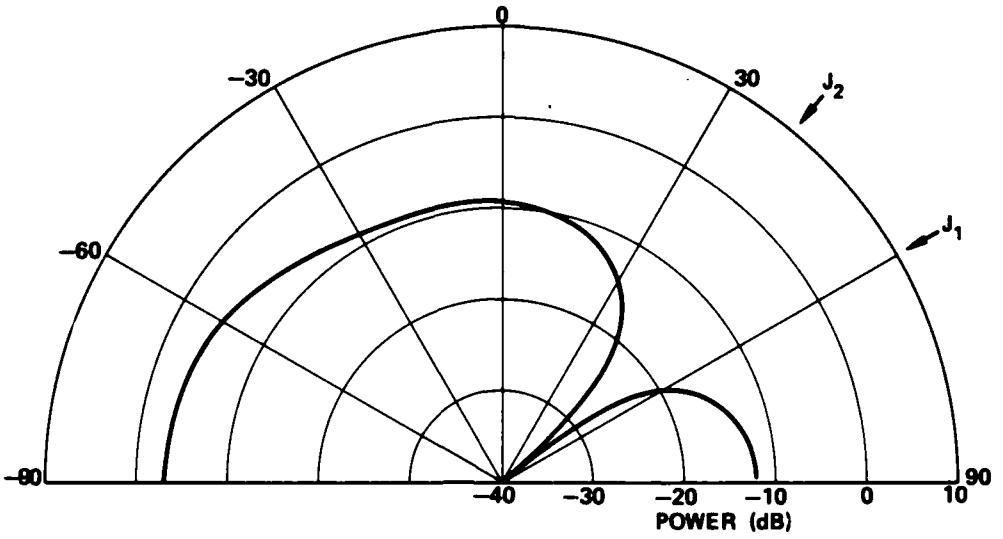

(d) J2 = 40 degrees.

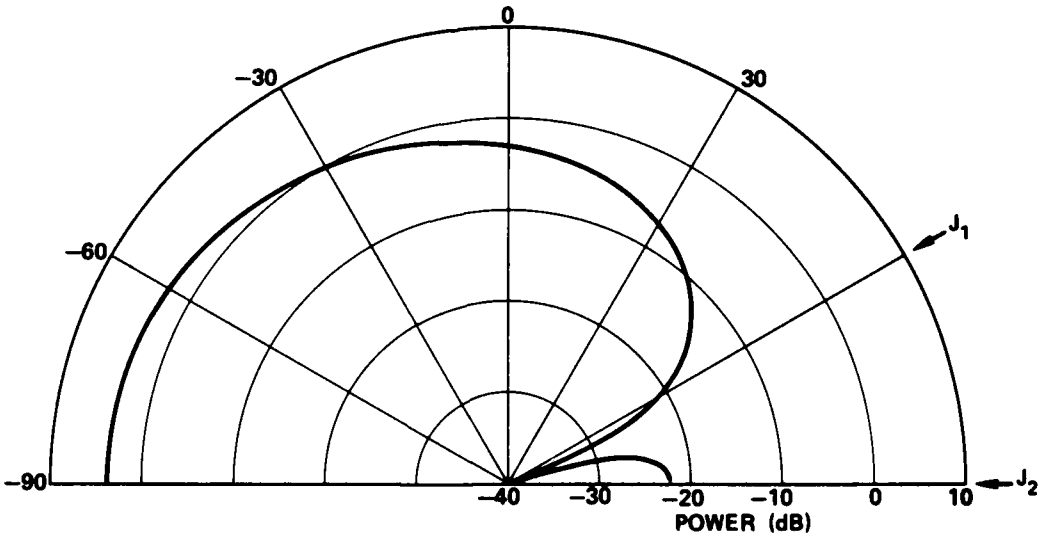

(e) J2 = 90 degrees.

FIGURE 20. (Contd.)

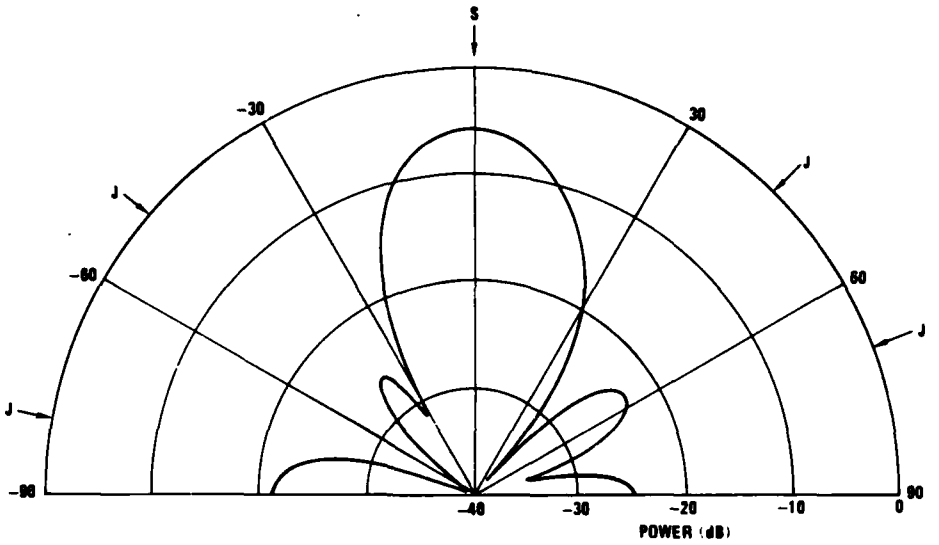

FIGURE 32. Adapted Antenna Pattern after Attempt to Null Four Jammers with a Nine-Element Array. Spacing = 0.2λ.

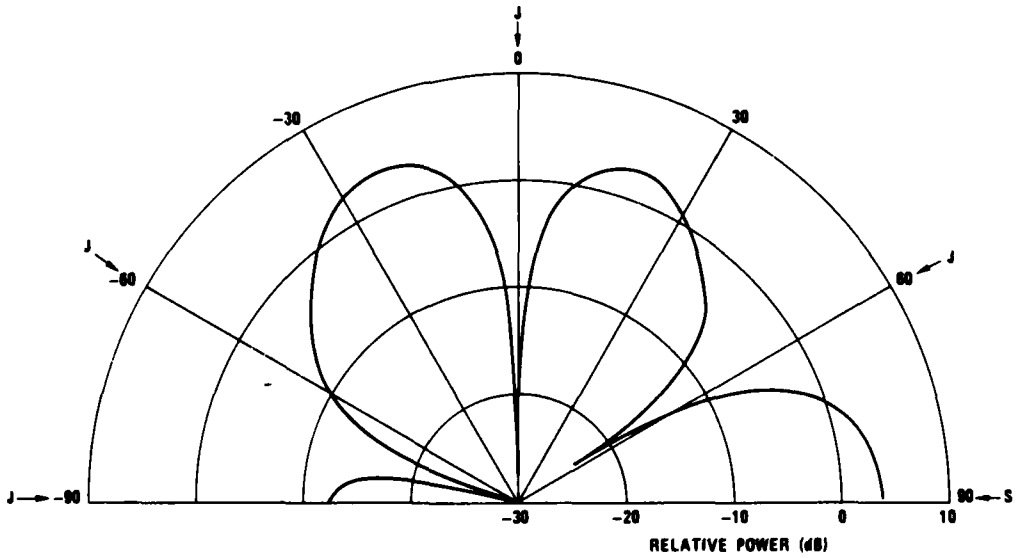

FIGURE 33. Adapted Antenna Pattern after Attempt to Null Four Jammers with a Nine-Element Array. Spacing = 0.2λ.

However, the addition of two elements to form the nine-element array from the seven-element array does give substantially improved performance when operating against three jammers. Figure 34 is a typical example taken from five jammer/desired signal cases examined. The adapted curves for both a nine-element array and a seven-element array are displayed. In both cases, the antenna pattern after 100 iterations is shown. The nine-element array clearly forms nulls that are narrower, deeper, and better aligned with the jammers as compared with the seven-element array. The final SJRs for the two cases were 25.5 dB and 9.0 dB for the nine- and seven-element arrays, respectively. We conclude that the two additional elements added to form the nine-element array from the seven-element array have added "partial" degrees of freedom; they assist in improving nulling performance, but are not adequate to allow a fourth jammer to be nulled.

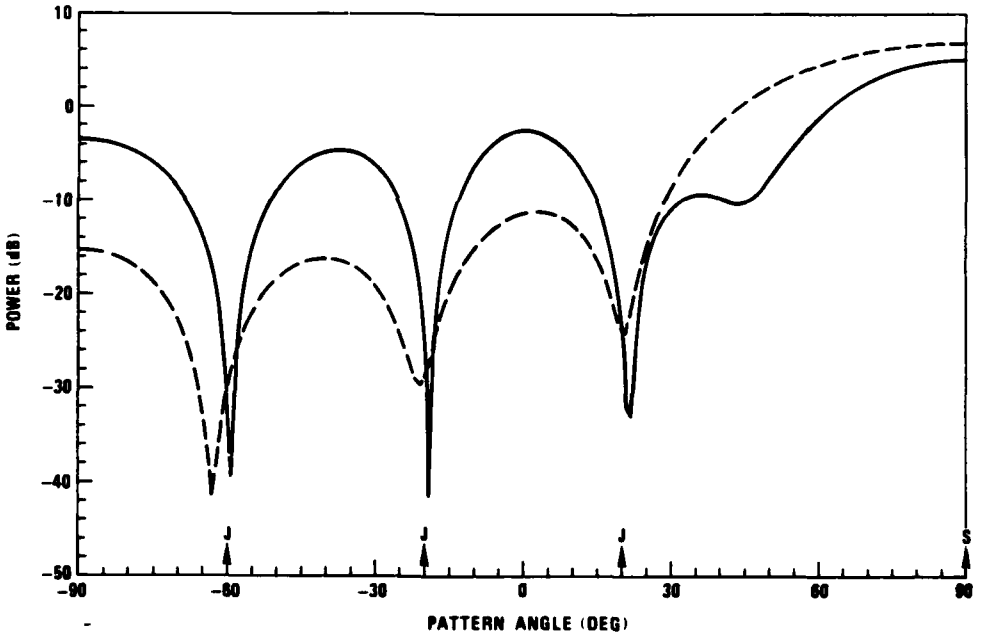

FIGURE 34. Adapted Antenna Pattern after Nulling of Three Jammers. Dash curve, seven elements; solid curve, nine elements. Spacing = 0.2λ.

DISCUSSIONS AND CONCLUSIONS

Table 1 is a compilation of the principal results of the simulations. The relation between the number of steerable nulls and the number of elements found for three, five, and seven elements is as expected. In any adaptive array, the formation of a null requires two degrees of freedom. In a conventional adaptive array (i.e., an array in which the output of each element is weighted in amplitude and phase, and outputs are summed in a summing element), the addition of one more element allows one more jammer to be nulled, since each element has two degrees of freedom (phase and amplitude). In the case of a reactively steered adaptive array (RESAA), however, each additional element adds only a single degree of freedom (the reactive termination value); therefore, two elements must be added to null one additional jammer.

Why, then, can a nine-element array not null four jammers? In a RESAA, the influence of a particular element on the antenna pattern decreases as the distance to the single active element increases, because the mutual coupling decreases with separation. Hence, at some point, adding elements to a linear array will reach a "point of diminishing returns." Clearly, for the linear dipole array, this point is reached when two elements are added to the seven-element array, since the nine-element array was unable to provide an additional null. A point that we were unable to address in this study is whether this behavior is related entirely to the distance between the parasitic elements, or whether limitations of the control algorithm with a greater number of controlled variables also caused difficulty in forming the additional null. The effect of distance can be assessed by investigating a planar array, so that a nine-element array can be formed by two five-element crossed arrays. A planar array simulation study is planned in FY-85.

The optimum element spacing was essentially independent of the number of elements in the array. (Before these simulations, we had made an educated guess that the optimum spacing would decrease as the number of elements increased, in order to attain tighter coupling to the relatively distant elements added to the array ends.) The three-element array investigation showed that the endfire and broadside spacings for best performance were 0.1λ and 0.25λ, respectively. The best spacing for five and seven elements, in which multiple jammers were present with random arrival angles so that near-endfire and near-broadside incidence occurred simultaneously, was about 0.2λ, which is approximately the mean of the three-element endfire and broadside values. There does not seem to be any obvious physical reason why this particular range of values is optimum.

The simulations showed conclusively that the power inversion (PI) mode only works for one or two jammers. For three jammers with seven or nine elements, a desired signal was necessary. The inability of the PI mode to work with three jammers is probably caused by the existence of local suboptimal minima in the control surface that "trap" the reactive loads during steepest descent. Successful operation in the desired signal (DS) mode indicates that the control surfaces for three jammers and a desired signal apparently either do not have as many local minima (so that the probability of a poor nulling solution is much lower), or the minima -- even though suboptimum -- give adequate nulling performance.

The nulling bandwidth showed essentially no dependence on the number of elements. The variation with element spacing was similar to the variation of the jammer power and signal-to-jammer power ratio (SJR) with element spacing; the bandwidth peaked at spacings of 0.1 to 0.3λ. The value within this range was about 0.2%. This value for the bandwidth resulted from adaptation to tone (single frequency) jammers. If jammers with a finite spectral extent were considered in the analysis and the simulations, the nulling bandwidth would undoubtedly be correspondingly wider.

The results of this study indicate that a RESAA is fundamentally a technique for small arrays (nine or less in a linear configuration). However, by using a RESAA as a subarray unit, larger arrays can be formed. The RESAA subarrays could then be summed and controlled in the manner of a conventional (fully driven) adaptive array.

REFERENCES

1. Naval Weapons Center. Reactively Steered Adaptive Array Using Microstrip Patch Elements at 4 GHz, by R. J. Dinger. China Lake, Calif., NWC, February 1983. (NWC TP 6421, publication UNCLASSIFIED).

2. ------. Closed Loop Adaptive Control of a 4.0 GHz Reactively Steered Microstrip Array: Experimental Results, by R. J. Dinger. China Lake, Calif., NWC, October 1983. (NWC TP 6481, publication UNCLASSIFIED).

3. R. J. Dinger and W. D. Meyers. "A Compact Reactively Steered Antenna Array," in 1980 Antennas Propag. Soc. Symp. Digest, PQ, Canada, 2-6 June, 1980. Pp. 312-15.

4. A. E. Zeger, L. D. Wismer, and R. J. Dinger. "Adaptive Control of Parasitic Elements," in Proceedings of the 1980 Adaptive Antenna Symposium, Vol. 1. Rome Air Development Center, Griffiss Air Force Base, N.Y., 1 December 1980. Pp. 87-105. (RADC Report No. TR-80-378, publication UNCLASSIFIED.)

5. Naval Research Laboratory. A Compact HF Antenna Array Using Reactively Terminated Parasitic Elements for Pattern Control, by R. J. Dinger and W. D. Meyers. Washington, DC, NRL, May 1982. (NRL Memo Report 4797, publication UNCLASSIFIED).)

6. R. F. Harrington and J. R. Mautz. "Reactively Loaded Directive Antennas," Syracuse University, Department of Electrical and Computer Engineering, September 1974. (Technical Report No. 1, publication UNCLASSIFIED.)

7. R. F. Harrington. "Reactively Controlled Directive Arrays," IEEE Trans. Antennas Propag., Vol. AP-26 (May 1978), pp. 390-97.

8. P. S. Carter. "Circuit Relations in Radiating Systems and Applications to Antenna Problems," Proc. IRE, Vol. 20, No. 6 (June 1932), pp. 1004-41.

9. G. A. Bekey and W. J. Karplus. Hybrid Computation. New York, Wiley, 1969.

10. H. H. Rosenbrock. "An Automatic Method of Finding the Greatest or Least Value of a Function," The Computer Journal, Vol. 3 (October 1960), pp. 175-84.

11. R. F. Harrington and J. Luzwick. "A Comparison of Optimization Techniques as Applied to Gain Optimization of a Reactively Loaded Linear Array," Syracuse University, Department of Electrical and Computer Engineering, February 1976. (Technical Report No. 1, publication UNCLASSIFIED.)

12. R. A. Monzingo and T. W. Miller. Introduction to Adaptive Arrays. New York, Wiley, 1980.

INITIAL DISTRIBUTION

8 Naval Air Systems Command
- AIR-03D, G. Heicke (1)
- AIR-330B, F. J. Lueking (1)
- AIR-330D, C. Caposell (1)
- AIR-330E, A. Glista (1)
- AIR-330R, J. Willis (1)
- AIR-340R, J. Smith (1)
- AIR-7226 (2)

5 Chief of Naval Operations
- OP-0941 (1)
- OP-0944 (1)
- OP-098 (1)
- OP-0986 (1)
- OP-987 (1)

8 Chief of Naval Research, Arlington
- ONR-200, J. O. Dimmock (1)
- ONR-210B, LCDR T. L. Swafford (1)
- ONR-250, CDR D. S. Siegal (1)
- ONR-414
  - D. Lewis (1)
  - R. Madan (1)
  - J. Wright (1)
- ONR-430, A. M. Diness (1)
- K. Davis (1)

4 Naval Electronic Systems Command
- Code 61A (1)
- Code 611, B. Hughes (1)
- Code 614, J. Cauffman (1)
- PME-109-20, R. Eisenberg (1)

5 Naval Sea Systems Command
- SEA-003 (1)
- SEA-09B312 (2)
- SEA-62R1
  - C. E. Jedrey (1)
  - T. Tasaka (1)

1 Commander in Chief, U.S. Pacific Fleet (Code 325)

1 Commander, Third Fleet, Pearl Harbor

1 Commander, Seventh Fleet, San Francisco

2 Naval Academy, Annapolis (Director of Research)

3 Naval Air Development Center, Warminster
- A. T. Cerino (1)
- H. H. Heffner (1)
- G. T. Pirrung (1)

1 Naval Ocean Systems Center, San Diego (P. Hansen)

8 Naval Research Laboratory
  Code 7500, J. R. Davis (1)
  Code 7550
    D. Himes (1)
    W. Meyers (1)
    L. Wagner (1)
  W. Gabriel (1)
  F. F. Kretschmer (1)
  C. M. Krowne (1)
  D. Townsend (1)
3 Naval Ship Weapon Systems Engineering Station, Port Hueneme
  Code 5711, Repository (2)
  Code 5712 (1)
1 Naval War College, Newport
1 Office of Naval Technology, Arlington (MAT-073)
1 Army Research Office, Research Triangle Park (J. W. Mink)
1 Harry Diamond Laboratories, Adelphi (A. .R. Sindoris)
1 Air Force Intelligence Service, Bolling Air Force Base (AFIS/INTAW, Maj. R. Lecklider)
2 Rome Air Development Center, Griffiss Air Force Base
  DCCR, J. A. Graniero (1)
  OCTS, V. Vannicola (1)
2 Rome Air Development Center, Hanscom Air Force Base
  R. Mailloux (1)
  H. Steyskal (1)
12 Defense Technical Information Center
1 General Atronics Corporation, Philadelphia, PA (L. R. Burgess)
3 Lincoln Laboratory, MIT, Lexington, MA
  J. T. Mayhan (1)
  K. Senne (1)
  A. Simmons (1)
1 New Mexico State University, Physical Science Laboratory, Las Cruces, NM (K. R. Carver)
2 Ohio State University, ElectroScience Laboratory, Columbus, OH
  R. T. Compton (1)
  A. A. Ksienski (1)
1 R. C. Hansen, Inc., Tarzana, CA (R. C. Hansen)
1 Stanford University, Department of Electical Engineering, Stanford, CA (B. Widrow)
1 Syracuse University, Department of Electrical and Computer Engineering, Syracuse, NY (R. A. Harrington)
2 University of California, Electrical Sciences and Engineering Department, Los Angeles, CA
  N. G. Alexopoulos (1)
  R. S. Elliott (1)
1 University of Colorado, Electromagnetics Laboratory, Boulder, CO (D. C. Chang)
1 University of Houston, Department of Electrical Engineering, Houston, TX (S. A. Long)
1 University of Pennsylvania, Moore School of Electrical Engineering, Philadelpia, PA (B. D. Steinberg)
1 University of Southern California, Department of Electrical Engineering (Systems), Los Angeles, CA (L. Griffiths)
1 Zeger-Abrams, Inc., Glenside, PA (A. E. Zeger)

END

FILMED

5-85

DTIC